WADC TECHNICAL REPORT 52-325, Part 1

AD 8776

ASNXRR

ELEVATED TEMPERATURE FATIGUE PROPERTIES OF SAE 4340 STEEL

W. J. TRAPP
MATERIALS LABORATORY

DECEMBER 1952

Statement A
Approved for Public Release

WRIGHT AIR DEVELOPMENT CENTER

2002 11040 76

NOTICES

ELEVATED TEMPERATURE FATIGUE PROPERTIES OF SAE 4340 STEEL

W. J. Trapp
Materials Laboratory

December 1952

RDO No. 614-16

FOREWORD

This investigation was conducted in the Structural & Design Data Branch of the Materials Laboratory, Directorate of Research, Wright Air Development Center, Wright-Patterson Air Force Base, Ohio, with Mr. W. J. Trapp acting as project engineer. It was initiated under the research and development project identified by Research and Development Order No. 614-16, "Fatigue Properties of Aircraft Structural Materials."

A B S T R A C T

This report presents the test procedures and results of a fatigue investigation at room and elevated temperatures on S.A.E. 4340 steel, oil quenched and tempered to 160,000 psi in the unnotched and notched condition. The notch used in the investigation is a 60° V-notch with 0.010" radius and 0.025" depth.

The results, which are presented in form of S-N diagrams, normal and nondimensional modified Goodman and stress-range diagrams, reveal the effect of temperature and stress-ratio on the unnotched and notched fatigue properties.

The fatigue tests were supplemented by stress-rupture and creep-rupture tests and by dynamic creep-measurements. The investigation was conducted at room temperature, 600°, 800° and 1000° F.

In general, the fatigue strength was found to decrease with increasing temperature at all stress levels and all stress-ratios except for the life times between 10^5 and 15×10^6 cycles in the notched condition, where at 600° the value is lower than at 800° and even lower than at 1000°, dependent upon stress ratio. This can probably be related to an increase in brittleness in the 600° region, which is also confirmed by the fact, that the notch sensitivity at 600° was found to be higher than at any of the other temperatures investigated.

The notch-sensitivity factor, based on maximum stress, is dependent upon temperature, stress-level and stress-ratio. It generally decreases with increasing stress level, increasing temperature and decreasing stress-ratio. The peak of notch-sensitivity is produced at completely reversed load for all temperatures.

The tests indicated that creep is dependent upon mean stress rather than upon maximum stress. Two distinct types of creep-time diagrams were obtained, determined by stress-ratio, mean stress and temperature. A fracture study revealed certain relations between the type of creep diagram and type of fracture, inter and transgranular.

A B S T R A C T (Cont'd)

Fatigue life at elevated temperature is not only dependent upon total number of cycles, but also upon time when creep is involved. The speed of loading (cyclic frequency), which determines the time available for creep and therefore the amount of creep must be considered. The ultimate failure in general is a combination of fatigue and creep, with the relative effects of each depending upon stress, stress-ratio, temperature and time.

PUBLICATION REVIEW

This report has been reviewed and is approved.

FOR THE COMMANDING GENERAL:
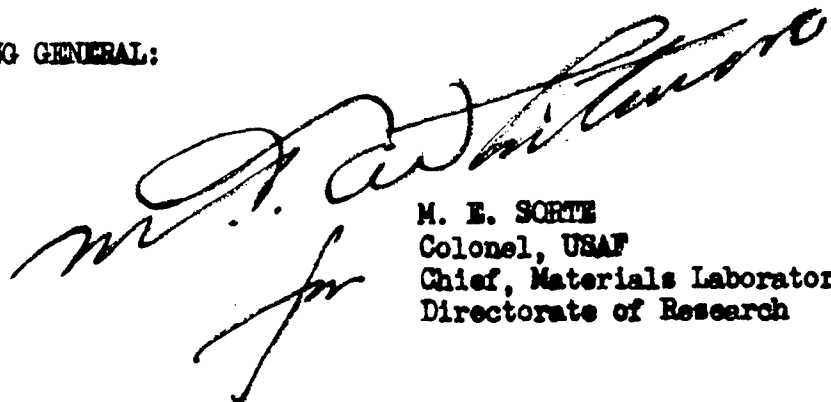
M. E. SORTE
Colonel, USAF
Chief, Materials Laboratory
Directorate of Research

TABLE OF CONTENTS

Page

LIST OF TABLES

TABLE

LIST OF ILLUSTRATIONS

FIGURE

LIST OF ILLUSTRATIONS (Cont'd.)

INTRODUCTION

There is little published information on the effect of mean stress on the axial loading fatigue properties, fatigue notch sensitivity and dynamic creep effects at elevated temperatures for steel. These properties were investigated in this project, and the results are presented in the form of modified Goodman and other diagrams.

MATERIAL AND PROCEDURE

The test material used was S.A.E. 4340 aircraft quality steel, conforming to Military Specification MIL-S-5000A. A chemical analysis disclosed the following results:

C	Mn	P	S	Si	Ni	Cr	Mo
0.414	0.79	0.024	0.014	0.29	1.76	0.77	0.27

It was produced in the form of rolled round bars of 1 1/8 inch diameter, all from the same heat. The cylindrical unnotched specimens were rough machined within 1/16 inch of the finished dimensions and heat-treated as follows: 1575°F. for 1 1/2 hours, quenched in oil, tempered at 1150°F. for 1 1/2 hours and air cooled. The specimens were given as nearly identical heat-treatment as possible. Although accomplished at different times because of the limited capacity of the furnace, the hardness produced was within two points Rockwell C for all specimens. After heat-treatment the specimens were turned to 0.400 inch diameter in the gage length of 1 3/4 inch with 1"-14 NF-3 threaded gripping ends (Figs. 4a and 4c). The threads have been ground to insure proper alignment of the specimens in the fatigue machine. All tool marks in the gage section of the specimens were removed by hand polishing. A surface finish was produced of about 10 micro-inches. The notched specimens were identically heat-treated and machined, except for the gage section, which was turned to 0.450 inch diameter and provided with a 60° circumferential groove, 0.025 inches deep with a 0.01 inch radius at the bottom (Figs. 4b and 4d). The groove was not polished since microscopic examination proved the surface finish to be identical with the one of the unnotched specimens. Since all possible care was given to the cutting of the notches (in selecting optimum feed and speed) it can be assumed that any residual stresses set up during maching operations were negligible.

The investigation was conducted in axial loading at room temperature, 600°, 800° and 1000°F. in a 20-ton Schenck fatigue testing machine (1). The frequency of the cyclic loading was between approximately 2000 and 2500 cpm. This frequency range is due to the fact that for this type fatigue machine the amplitude of the cyclic load is controlled by the speed of an eccentric which excites the dynamic loading spring. The specimen grips are made out of the low heat conducting Inconel X material. They are water cooled in order to avoid temperature influence on the dynamometer, loading spring system and

the creep measurements. The specimens are fitted with lock nuts, which were processed very carefully in cutting the thread and facing the ends as accurately as possible, so that no bending stresses would be applied to the specimen by tightening the nuts.

The stress distribution in the gage section of each specimen was checked with Huggenberger Extensometers before starting each test. The maximum deviation from the average strain was found not to be higher than 2%. A more thorough check was conducted with SR-4 strain gages on a specimen picked at random. Three gages were mounted at each end of the gage section on its periphery 120° apart. The maximum deviation in the periphery of one end was found to be 1.45%, in the other end 1.63%. The difference between the average stresses in the peripheries of the two ends was found to be 0.7%. The furnace is a split type provided with three separate heating coils in order to control temperature distribution in the axial direction. The temperature gradient over the gage length of the specimen is maintained within ± 5° F.. at 1000°F.; the horizontal arrangement of the furnace in the fatigue machine aids in attaining a uniform temperature. The temperature control thermocouple is fixed to the specimen itself. In this way the desired temperature is reached automatically and maintained very closely and any temperature change in the specimen, for instance, that due to heat generation by damping in the material, is balanced out without overshooting. A Leeds-Northrup Micromax recording controller ranging from 0 to 2000° F. controls the testing temperature with an accuracy of ±2° at 1000° F.

The dynamic creep measurement was accomplished by measuring the gripping head travel. The movement of the head is transferred to a leaf spring (Fig. 2) from which the deflection or strain, respectively, is picked up by wire gages, amplified and recorded on a Brown Electronik Recorder. This equipment, which has been especially developed for this purpose, permits measurement of head travel with an accuracy of 0.0001 inch. Although the measurement includes the complete gripping system, measurements with Huggenberger extensometers on the gage section of the specimen indicated that the creep in the specimen is obtained with an accuracy of 1%. This accuracy is maintained for all temperatures tested by water cooling the gripping system and keeping it at a constant temperature during the test. To determine the creep in the specimen by using the head travel it is necessary to determine the effective gage length, which takes into consideration the creep in the fillet section of the specimen. The effective gage length was calculated by assuming that the creep-rate law is a hyperbolical sine function (4) and by using a graphical integration of strain over the straight section and fillet section of the specimen. This procedure was conducted for each specimen. The range of the effective gage lengths was between approximately 110 and 130% of the actual machined gage length.

The creep-rupture tests were executed in a Baldwin-Southwark Creep-rupture testing machine with a 20,000 lbs. capacity, equipped with an automatic creep-time recorder. All creep data are obtained in the form of time-elongation curves for constant load and temperature.

The static tests were conducted in a 20,000 lbs. capacity Olsen testing machine. The stress-strain diagrams at all four temperatures were obtained with a Templin Stress-strain recorder. The room temperature test was conducted with an Olsen strain gage on the specimen at the same time, as a check. The rate of loading was kept constant according to the elongation of 0.05 inch/min.

RESULTS AND DISCUSSION

Values of unnotched and notched static and fatigue properties for different temperatures are given in Tables 1 and 2. Fig. 5 shows the stress-strain diagrams of one of three specimens tested at each temperature, for room temperature, 600°, 800° and 1000°F., which demonstrate increasing ductility of the material with temperature, indicated by increasing strain at a given stress with increasing temperature. Ultimate Tensile Strength, Yield Strength, Proportional Limit and Modulus of Elasticity drop gradually with temperature.

The fatigue test results are presented in form of S-N diagrams for the different stress ratios, unnotched and notched, up to a life of 15 million cycles. As an extract of the whole investigation, normal and dimensionless modified Goodman type diagrams and alternating stress-mean stress diagrams are presented, which are considered the best and most efficient condensation of the results for the designer.

In Figure 6 are given the S-N diagrams for room temperature, 600°, 800° and 1000°F. for tensile loading zero to maximum in unnotched condition. The curves follow the general trend of decreasing fatigue strengths with increasing temperature, but at 800° and even more at 1000°, the diagrams produce a change in characteristic. A steeper slope at the low stress level indicates a higher effect of temperature in this region. The fatigue strength for 15×10^6 cycles is reduced to 83% of the room temperature value at 600°, to 71% at 800° and to 56% at 1000° F. This higher effect of temperature is connected with the phenomena of creep, as well as fatigue, causing failure. This is discussed in detail later. The solid points plotted in Figure 6 represent specimens with extraordinary large inclusions found in the failure section of the specimens (details see page 10). The low points are not considered in drawing the curves because there were found no inclusions of anywhere near this size in a subsequent lot of material submitted by Republic Steel Corporation for comparison. It is felt that the lot which produced the large inclusions is an exception which probably will not occur in present production.

Figure 7 presents the S-N curves for completely reversed loading at room temperature, 600°, 800° and 1000° F. The diagrams indicate little effect of the temperature at 600° and 800°, but a comparatively considerable reduction at 1000° F. The fatigue strength for 15×10^6 cycles is reduced to 91% of the room temperature value at 600°, to 86% at 800° and to 56% at 1000°F. Since there is negligible opportunity for permanent creep in completely reversed loading, stress-ratio A=∞, (see Figure 37) the failure is entirely fatigue controlled at all the temperatures. Whereas in any loading where the mean stress is other than zero, the ultimate failure at elevated temperatures is a

combination of fatigue and creep. The relative effects of creep and fatigue depend upon temperature, stress and stress-ratio. No correlation between these factors and the type of failure has been found. Efforts in this direction are being made in the fracture studies, which are discussed later.

The comparatively low fatigue strengths at 1000° might be connected with the extremely low proportional limit found at this temperature. As seen in Figure 5, the proportional limit decreases as temperature increases.

Figure 8 shows the S-N diagrams for high constant mean stress at each temperature level in unnotched condition. The individual mean stresses have been selected to produce the most complete Goodman diagram possible with the limited number of specimens available, since no more material of the same heat could be procured.

The number of cycles which are considered to represent the endurance limit for steel at room temperature is 10^7. But for a sufficiently high temperature and mean stress a definite endurance limit seems to be lacking, the S-N curve continues to drop. As long as any indication of creep is present, failure can be expected even at number of cycles higher than 15×10^6 cycles, the maximum cycles used in this investigation.

In Figure 9 the Goodman type diagrams for different temperatures in unnotched condition for 15×10^6 cycles are presented. The peaks of the diagrams, which are the points of maximum mean stress at the different temperatures, represent the static creep-rupture values for 120 hours, which is the same time the dynamic tests have been run, namely 15×10^6 cycles. No creep-rupture tests were made for 120 hours at room temperature since tests over several hours did not produce any amount of creep and reduction in strength.

The normally used short time ultimate tensile strength value is not suitable for this diagram, because of the considerable amount of creep involved with increasing temperature. The diagrams Figure 10 to 13 are the S-N diagrams and modified Goodman diagrams for the notched condition. The S-N diagrams, Figures 10 and 11, produce the usual steep slope in the high stress level compared to unnotched. The negative influence of temperature of fatigue strength decreases considerably with number of cycles compared to unnotched. At 10^7 cycles for zero to maximum load the fatigue strength at 800° and 1000° is reduced to 71% and 56%, respectively, of the room temperature value in unnotched condition, whereas in the notched condition it is reduced to only 85% and 66% respectively. For completely reversed load, this trend is even more distinct. The values are 86% and 56% for unnotched and 93% and 87% for the notched at 800° and 1000° respectively. For 600° the behavior is different compared to 800° and 1000°. The fatigue strength at the low stress level is lower than at 800° for zero to maximum and even lower than 1000° for completely reversed.

The slenderness of the modified Goodman type diagram in Figure 13 for notched condition compared to the diagram for unnotched condition in Figure 9 demonstrates the effects of the notch on fatigue for different stress ratios.

The effect of temperature, stress level and stress ratio on notch sensitivity can be observed in Figures 34 to 36. There is no generally valid correlation between these three factors and notch sensitivity, but for lower stress levels and all but the lowest stress ratios, the notch sensitivity at 600° F. is the highest, while at 800° and at 1000° the notch sensitivity is lower than at room temperature. The notch sensitivity is defined as:

$$q' = \frac{K_f - 1}{K_t' - 1}$$

where K_f is the fatigue strength reduction factor and K_t' is the "technical" stress concentration factor, derived from H. Neuber's "Theory of Notch Stresses" (2). The factor q' was used, based on K_t', rather than the factor q, based on K_t, because the value of K_t', which takes into consideration the effect of the flank angle of the notch comes closer to the actual fatigue reduction factors found in the investigation (see TABLE 2) than K_t, which is the theoretical elastic stress concentration factor. For the notch used in this investigation (see Figure 4) $K_t' = 1.8$ and the corresponding theoretical stress concentration factor $K_t = 3.3$ therefore $q = q' \times 0.348$.

The nondimensional modified Goodman diagrams in Figures 14 to 23 for the unnotched and notched conditions at different temperature and stress levels reveal, in general, the trend of increase in ductility with increasing temperature, but this is not true for all stress ratios for either the unnotched or notched condition. The fatigue data for the unnotched condition, for all stress ratios and life times at all temperatures, are above the modified Goodman straight line, which can be expressed as:

$$\frac{S_a}{S_e} = 1 - \frac{S_m}{S_c}$$

S_a is the allowable alternating stress for specified lifetime or number of cycles and for specified mean stress S_m. S_e is the experimental fatigue strength at the same life time for completely reversed stressing. S_c is the experimental static creep-rupture strength (or tensile strength at room temperature) for specified lifetime converted to hours. The data at 1000° F. is the farthest above the line. These results are an indication of ductility and show that the allowable stresses obtained by the use of the modified Goodman line are conservative for these conditions. For the notched condition the data at all temperatures for 15×10^6 cycles are on or above the modified Goodman line, although closer to the line than for the unnotched condition. For higher stress levels the notched data fall below the line in some instances.

In Figures 24 to 33 stress range diagrams (alternating versus mean stress) for unnotched and notched conditions are presented. The diagrams reveal that the mean stress is more effected by temperature than the alternating. This effect is more distinct in the unnotched than in the notched condition and more at low than at the high stress level. For the notched condition the curves display an extreme flatness, especially at the low stress level, and even a concavity for all temperatures except for 1000° F., which indicates that a small increase of the dynamic load greatly reduces the mean load carrying capacity at the low stress level or region of large number of cycles.

In Figures 34 and 35 plots are made of the notch sensitivity ,q', as function of life or stress level for the two different stress ratios $A = \infty$ and $A = 1$. It is indicated that at all temperatures, but room temperature and 600°F. for the stress ratio $A = \infty$, the notch sensitivity displays a maximum at a stress level corresponding to a number of cycles between 10^5 and 10^6. The highest values of notch sensitivity were found at 600°F. except for the highest stress level, where the notch sensitivity was higher at 800°. Figure 36 demonstrates the influence of stress ratio on notch sensitivity at different temperatures. The trend is decreasing notch sensitivity with decreasing stress ratio at all temperatures tested with the exception between $A = \infty$ and $A = 1$ at 1000° F. The peak of notch sensitivity is indicated at stress ratio $A = \infty$ for all temperatures except for 1000° F.

In Figures 37 and 38 a few creep-time diagrams are presented, which were selected to demonstrate the main properties found and to show the two different characteristic creep curves, which we shall call the static type and the dynamic type. They are dependent on ratio of alternating to mean stress, magnitude of mean stress, and temperature. The static type is similar to the normal creep rupture curve and leads to the typical creep rupture failure, whereas the dynamic type produces comparatively little creep in the second stage and practically no third stage creep at all. It leads from the second stage of creep abruptly to the typical fatigue type failure.

Figure 37 demonstrates the changeover in characteristic of the creep-time curve from static to the dynamic type for 1000° F. The creep-time curves for five mean stresses are plotted and it is seen that the change is from the normal static type (or creep-rupture) at $S_m = 53,000$ psi to the completely dynamic type (or fatigue). This range of stress extends from static loading ($A = 0$) to completely reversed loading ($A = \infty$). The creep curves for $S_m = 50,000$, $S_m = 42,000$ and $S_m = 34,250$ psi show combinations of static and dynamic characteristics in varying degrees. Between $S_m = 54,000$ and $S_m = 42,000$ psi there is a change from mostly static to mostly dynamic characteristics, as the curve for $A = 0.26$ has a third stage creep, while the curve for $A = 0.85$ has no third stage and shows the dynamic type of failure. This diagram indicates that creep is highly dependent on mean stress rather than on maximum stress.

At low temperatures the effect of mean stress is different in that the type of creep characteristic does not change until the stress is close to the yield point. This effect of temperature is due to the different types of stress-strain diagrams at different temperatures, as seen in Figure 5. The change from dynamic type of creep curve towards the static type appears to start at some constant ratio of stress to strain regardless of temperature. From here on higher mean stresses or lower stress-ratios produce a creep diagram rather similar to the static creep curve. This indicates that down to a certain stress-ratio as well as up to a certain temperature, fatigue contributes most to cycles or time to failure, beyond this region creep is increasingly of more influence than fatigue. The change from dynamic towards static type of curve is more rapid at low temperatures because the stress-strain ratio changes suddenly, as seen by the sharper knee in the room temperature stress-strain curve.

This effect of temperature is seen in Figure 38 where two creep-time curves of two stress-ratios each for room temperature and 1000° F. are plotted. The change from low to high mean stress (from high to low stress-ratio) at room temperature does not cause any change in characteristics, while at 1000° F. the creep curve changes from dynamic to static type. No third stage of creep is noticeable at room temperature, but at 1000° F. , one is present similar to a normal static creep diagram. For the stress-ratio A = 1.0 only very little difference in minimum creep-rate and no third stage of creep was found at either temperature.

The ratio of minimum creep rate at different temperatures for instance for room and 1000° F. corresponds approximately with the ratio of plastic strain in the stress-strain diagrams at the respective points of stress.

A certain relation between characteristics of the creep diagrams and the type of fracture could be found. Although grain boundaries are very difficult to detect in S.A.E. 4340 steel and only a limited number of dynamic creep diagrams are available, the following trends have been noted:

(1). The dynamic type of creep diagram seems to correspond with a transgranular fracture at all temperatures and in some cases with partly transgranular and partly intergranular fracture dependent upon stress-ratio.

(2). The static type of creep diagram, when in conjunction with a great amount of strain (necking of the specimen) at room temperature, indicated transgranular fracture, but with decreasing strain and increasing temperature an intergranular fracture is more likely to occur. However, this question needs further investigation and this has been initiated. Because of the difficulty in locating the grain boundries in S.A.E. 4340 steel, it has been decided to continue the fracture studies on a titanium alloy, where grain boundaries are much easier to detect.

In Figure 39, a fatigue fracture is shown with a spherical inclusion of an aluminum oxide-silicate composition in center (see page 5). These

inclusions were found occasionally during this investigation. When present they were always the nucleus for the fatigue failure, which expanded radially to a circular area. The size of this circular area depended upon the stress ratio. The remaining area failed statically. These large size inclusions, which in some cases were found to be 0.003 inch in diameter, were discovered undamaged only in 0 to maximum loading or in creep-rupture and only at elevated temperatures in the unnotched condition. In other tests the inclusions were no longer spherical, but were broken up. Specimens which were found to have large size inclusions are marked in Figure 6 and show considerable reduction in fatigue strength. Microexamination of the specimens made by the metallurgical laboratory of the Republic Steel Corporation revealed some fine dispersed globular nonmetallic inclusions throughout the matrix of the steel. In the petrographic examination, the inclusions proved to be carborundum (Al_2O_3) crystals with silicate glass corresponding most likely to anorthite, a $C_aO-Al_2O_3-SiO_2$ composition, which is probably a deoxydation product rather than a product of refractory erosion. It had to be expected, that besides the great reduction in fatigue caused by the large size inclusions, the results of the whole investigation would be unfavorably influenced by smaller size inclusions. Check tests with supposedly clean material, submitted by Republic Steel Corporation especially for this purpose, revealed negligible influence in this respect. However, in a few specimens of this material, submitted by Republic Steel Corporation, small inclusions of the same appearance were found, which may indicate that the SAE 4340 steel in general is permiated by this composition. The effect of the inclusions on fatigue increased with temperature. At room temperature and at 600° F. all specimens failed within the normal scatterband and no large size inclusions were found present in the fracture area. At 800° and 1000° F. specimens found to have inclusions in the fracture area failed far below the normal scatterband.

It is realized that, even at about the same hardness, treatments for 4340 steel other than quenched and tempered may produce better high temperature properties such as at 1000° F. and higher. The following data on 4340 steel exemplify this:

	NORMALIZED *(5)		OIL QUENCHED AND TEMPERED	
	Tested at room temperature	Tested at 1000° F.	Tested at room temperature	Tested at 1000° F.
Tensile strength, psi	168,000	99,000	158,500	80,700
Yield strength, 0.2% offset	106,000	86,500	146,900	62,600
Creep-rupture strength, at 100 hours, psi	———	48,000	———	40,000**
Elongation, % in 4D	14	18	15	20

**120 hours
*First Treatment: N. at 1750 F. + T. 2 Hrs. at 1200° F.
  Second Treatment: N. at 1750° F.
Specimens cut from turbine disk.

CONCLUSIONS

1. Within the temperature range investigated the unnotched fatigue strength decreases as the temperature increases at all stress levels and stress-ratios. The notch sensitivity is dependent upon temperature, stress level and stress-ratio, but no generally valid correlations were found. The highest notch sensitivities of all temperatures investigated are at 600° F. While for low stress levels, the notch sensitivities at 800° F. and 1000° F. are lower than at room temperature and 600° F., the sequence changes with increasing stress level, and the highest notch sensitivity is at 800° F. Also, the influence of temperature on notch sensitivity decreases in general for all temperatures with increasing stress level.

2. Creep is more dependent upon mean stress than upon maximum stress. The failure characteristics change from pure fatigue to pure creep as the stress ratio decreases from $A = \infty$ to $A = 0$ at elevated temperatures. Two distinct types of creep-time diagrams are obtained for high and low stress-ratios. The cause of this is seen in a study of fractures, which indicates that at high stress-ratios the failure is transgranular at all temperatures, while at low stress ratios, the failure is intergranular at room temperature, becoming transgranular as the temperature increases.

3. At elevated temperatures creep occurs under dynamic loading at all stress-ratios except $A = \infty$. At stress-ratio $A = \infty$ the ultimate failure is pure fatigue, but at all other stress-ratios the ultimate failure may be fatigue or creep depending upon the relative magnitude of the effects of stress, temperature and time.

4. Life at elevated temperature fatigue is dependent not only on the stress and number of cycles, but also on time, more or less according to stress-ratio. This means, in selecting design stresses, two limitations must be considered, fracture shall not occur and the total deformation shall not be excessive.

5. The speed of loading (cyclic frequency) must be considered at elevated temperatures since it determines the length of time in which creep may occur.

REFERENCES

1. AF Technical Report No. 5623. "Six Ton Schenck Fatigue Testing Machine."

2. H. Neuber: "Theory of Notch Stresses." The David W. Taylor Model Basin Translation 74.

3. George V. Smith: "Properties of Metals at Elevated Temperatures." McGraw-Hill 1950.

4. A. Nadai: "The Influence of Time upon Creep. The Hyperbolic Sine Creep Law." Stephen Timoshenko Anniversary Volume 1938.

5. Sixth Progress Report on: "Four Low-Alloy Steels for Rotor Disks of Gas Turbines in Jet Engines," by A. Zonder and J. W. Freeman, University of Michigan, Project No. M 903, WADC Contract No. AF 33(038)-13496.

TABLE 1

Static, Creep-Rupture and Fatigue Properties
of S.A.E. 4340 Steel, Heat-Treated to 160,000 psi.

UNNOTCHED

| Temp. °F | Tensile Properties ① | | | | Creep-Rupture Properties ② | | | Axial Loading Fatigue Properties ② | | | |
	Ult.T.S. psi	Y.S. 0.2% Offset psi	Elong. in 4D %	Reduct. of Area %	Creep Rupture Strength psi	Elong. in 4D %	Reduct. of Area %	Tension 0 to Maximum psi	Completely Reversed psi	Other Stress Ratios Mean Stress psi	Alternating Stress psi
Room	158,500	146,900	15.0	52.4	—	—	—	+115,000	±70,000	+120,000	±25,000
600	152,800	121,400	19.3	59.0	145,000	15.2	55.0	+ 96,000	±64,000	+ 80,000	±40,000
800	125,000	104,500	16.3	67.9	104,000	21.8	68.7	+ 82,000	±60,000	+ 95,000	±30,000
1000	80,700	62,600	20.6	78.6	40,000	20.0	30.0	+ 65,000	±39,000	+ 40,000	±20,000

Note: ① Average of three specimens.

② Fatigue Strength and Creep-Rupture values are at 15 x 10⁶ cycles or 120 hours respectively.

TABLE 2

Static, Creep-Rupture and Fatigue Properties of S.A.E. 4340 Steel, Heat-Treated to 160,000 psi.

Temp. °F.	Tensile Properties ①			NOTCHED ② Creep-Rupture Properties			Axial Loading Fatigue Properties ②					
	Ult.T.S. psi	Reduct. of Area %	Static Notch Factor K	Creep Rupture Strength psi	Reduct. of Area %	Creep Notch Factor K	Tension 0 to Maximum psi	Completely Reversed psi	Fatigue Strength Reduction Factor K_f Tension 0 to Maximum	Compl. Reversed	Other Stress Ratios Mean Stress psi	Altern. Stress psi
Room	190,000	11.2	0.83	—	—	—	+57,500	±30,000	2.0	2.3	+150,000	± 6,500
600	176,000	17.2	0.87	173,000	11.8	0.84	+43,000	±25,000	2.2	2.6	+120,000	±12,500
800	154,900	24.3	0.81	120,500	25.8	0.87	+49,000	±28,000	1.7	2.1	+ 74,000	±19,000
1000	98,400	33.2	0.82	33,000	6.0	1.03	+37,500	±26,000	1.4	1.5	+ 28,000	±14,000

Note:

① Average of three specimens.

② Fatigue Strength and Creep-Rupture values are at 15×10^6 cycles or 120 hours respectively.

TABLE 3

Creep-Rupture Data

UNNOTCHED

Temperature °F.	Rupture Stress psi	Rupture Time Hours	Elongation in 4D %	Reduction of Area %
600	144,000	176.5	15.0	53.2
600	146,500	35.7	15.5	57.2
600	151,000	0.25	17.5	61.3
800	101,800	151.8	20.5	64.2
800	109,000	30.5	22.6	71.9
800	118,000	2.3	16.8	71.7
1000	43,000	84.5	32.4	30.2
1000	46,000	17.8	42.0	55.5
1000	52,000	9.0	31.5	——

NOTCHED

Temperature °F.	Rupture Stress psi	Rupture Time Hours	Reduction of Area %
600	172,000	200.0	11.7
600	185,500	0.25	14.0
600	175,000	39.0	11.9
800	120,000	100.0	25.7
800	126,000	42.0	25.5
800	140,000	2.3	27.0
1000	35,000	65.0	6.4
1000	50,000	9.3	8.2
1000	60,000	5.5	8.3
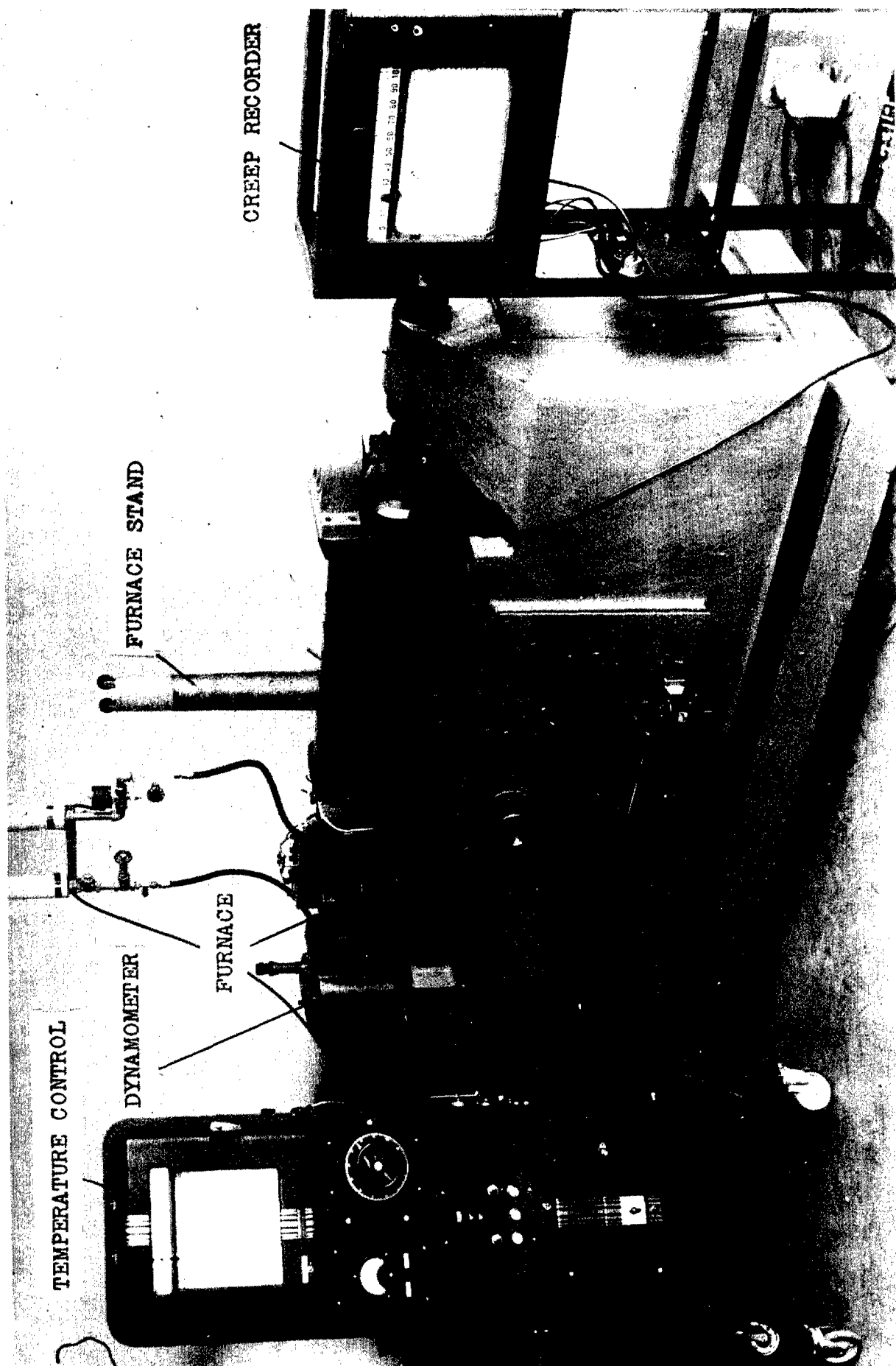
FIG. 1. EQUIPMENT FOR ELEVATED TEMPERATURE FATIGUE TESTING
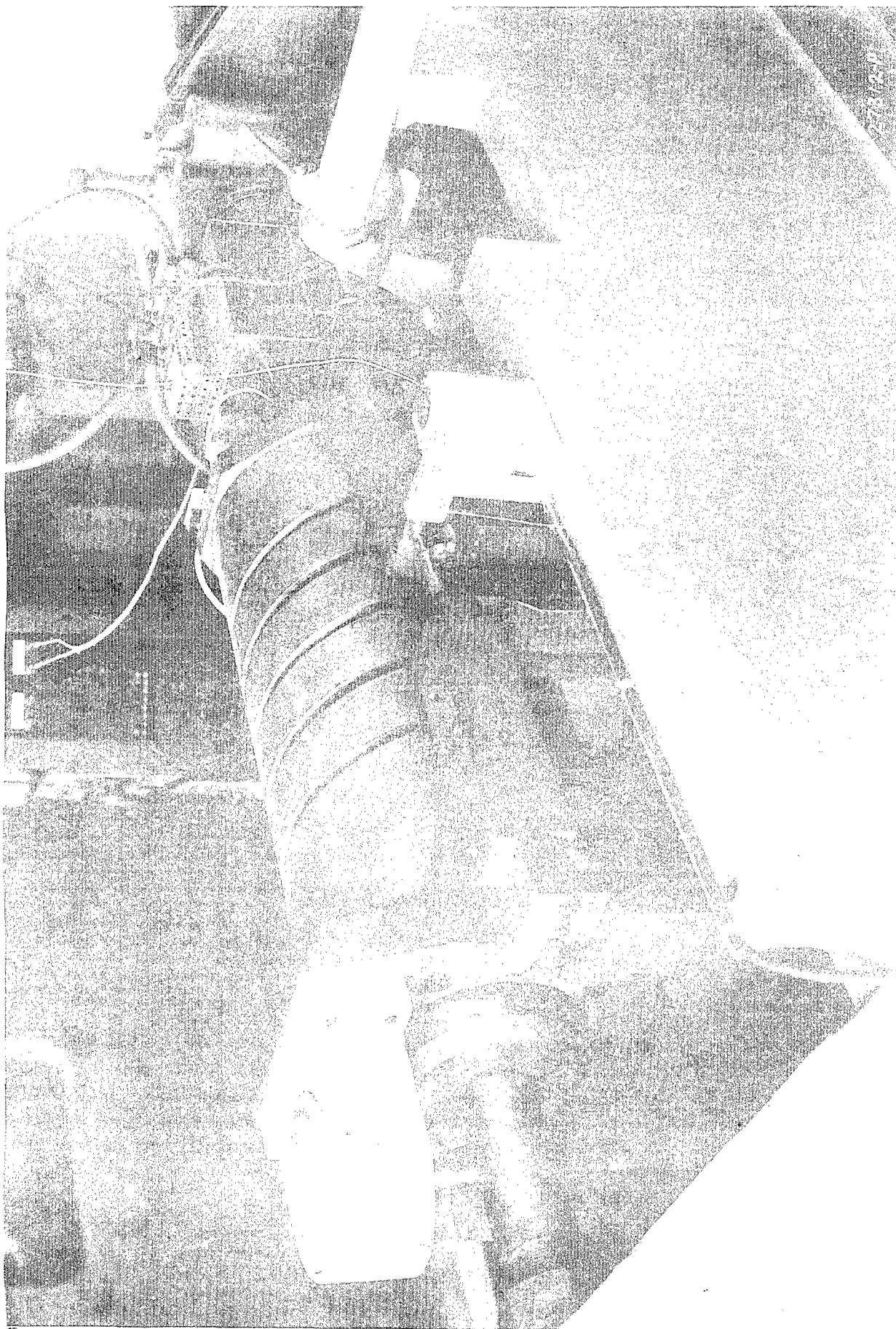
FIG. 2. FATIGUE MACHINE WITH DYNAMIC CREEP PICKUP
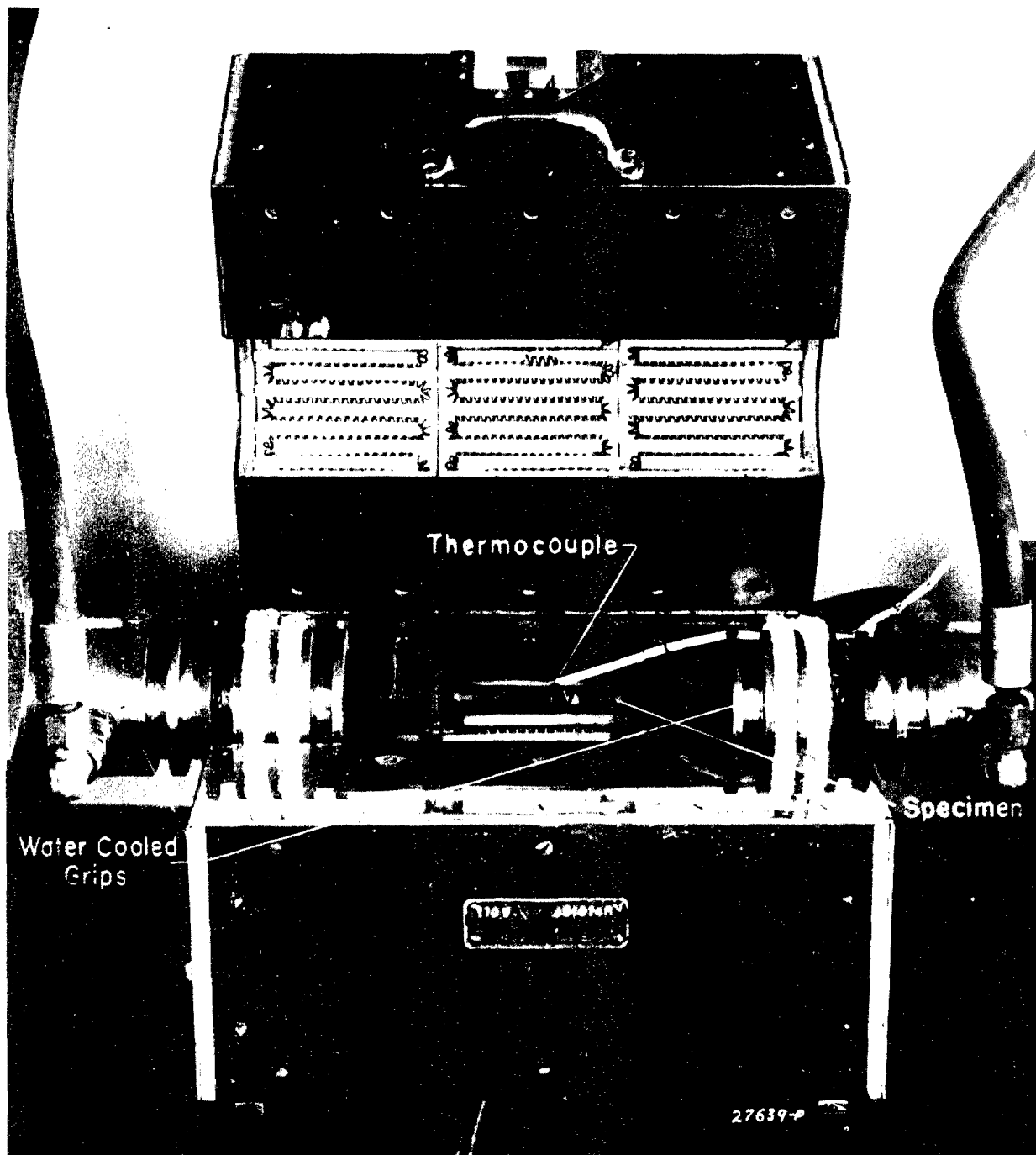
FIG. 3. FURNACE WITH SPECIMEN
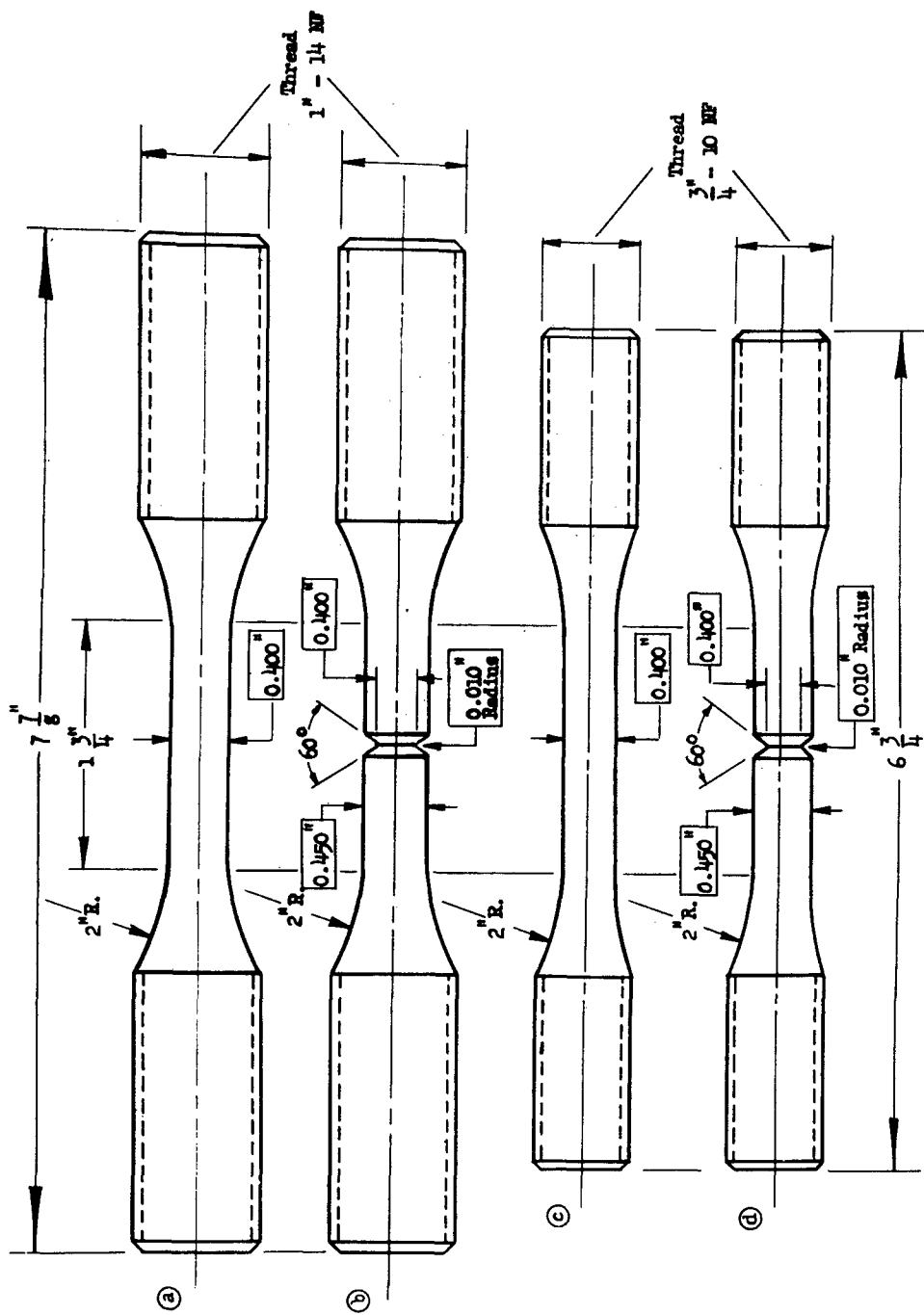
FIG. 4. SPECIMENS, (a) (b) - FATIGUE AND STRESS RUPTURE

(c) (d) - CREEP RUPTURE
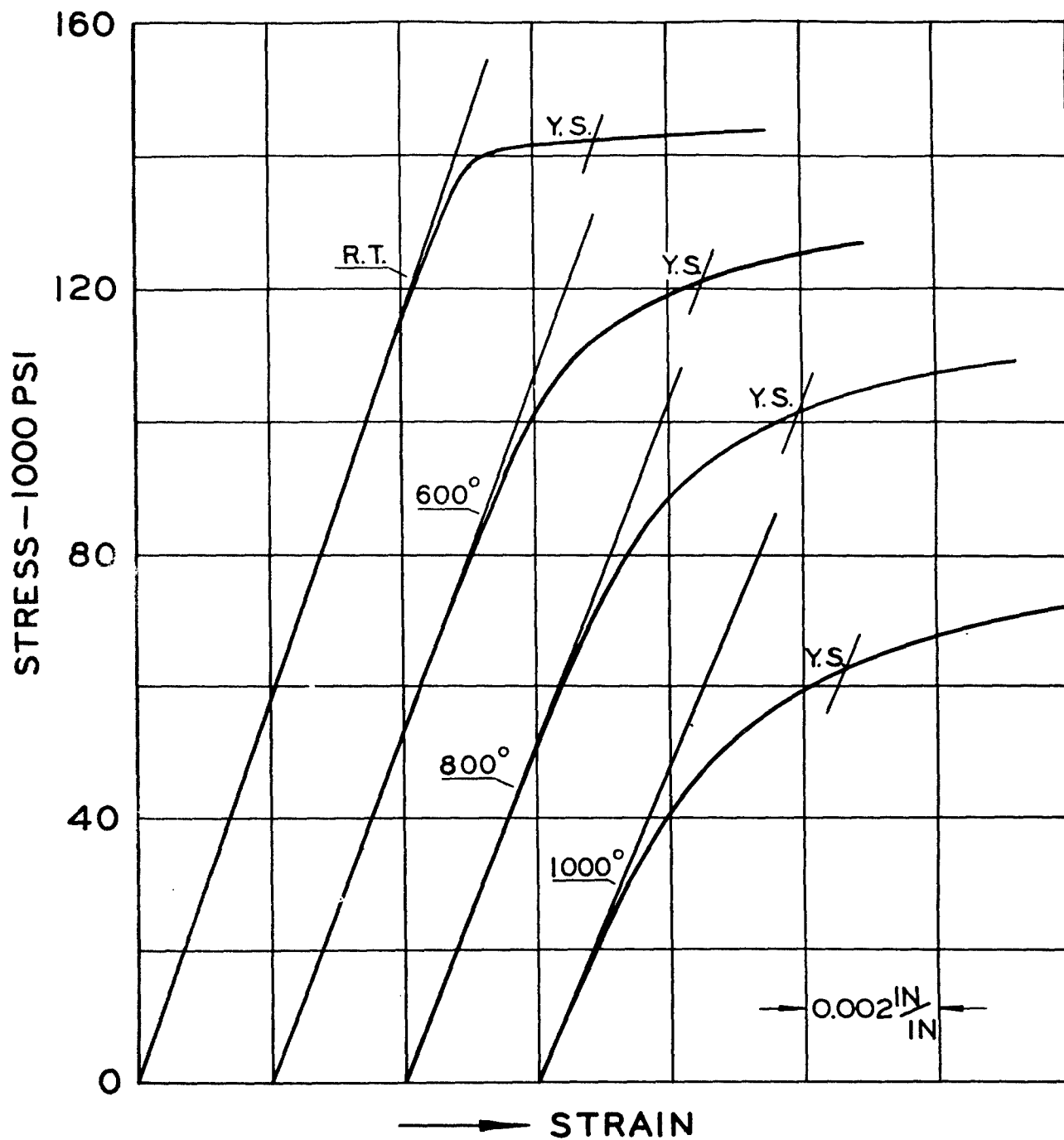
FIG. 5. STATIC STRESS-STRAIN DIAGRAMS FOR ROOM AND ELEVATED TEMPERATURES
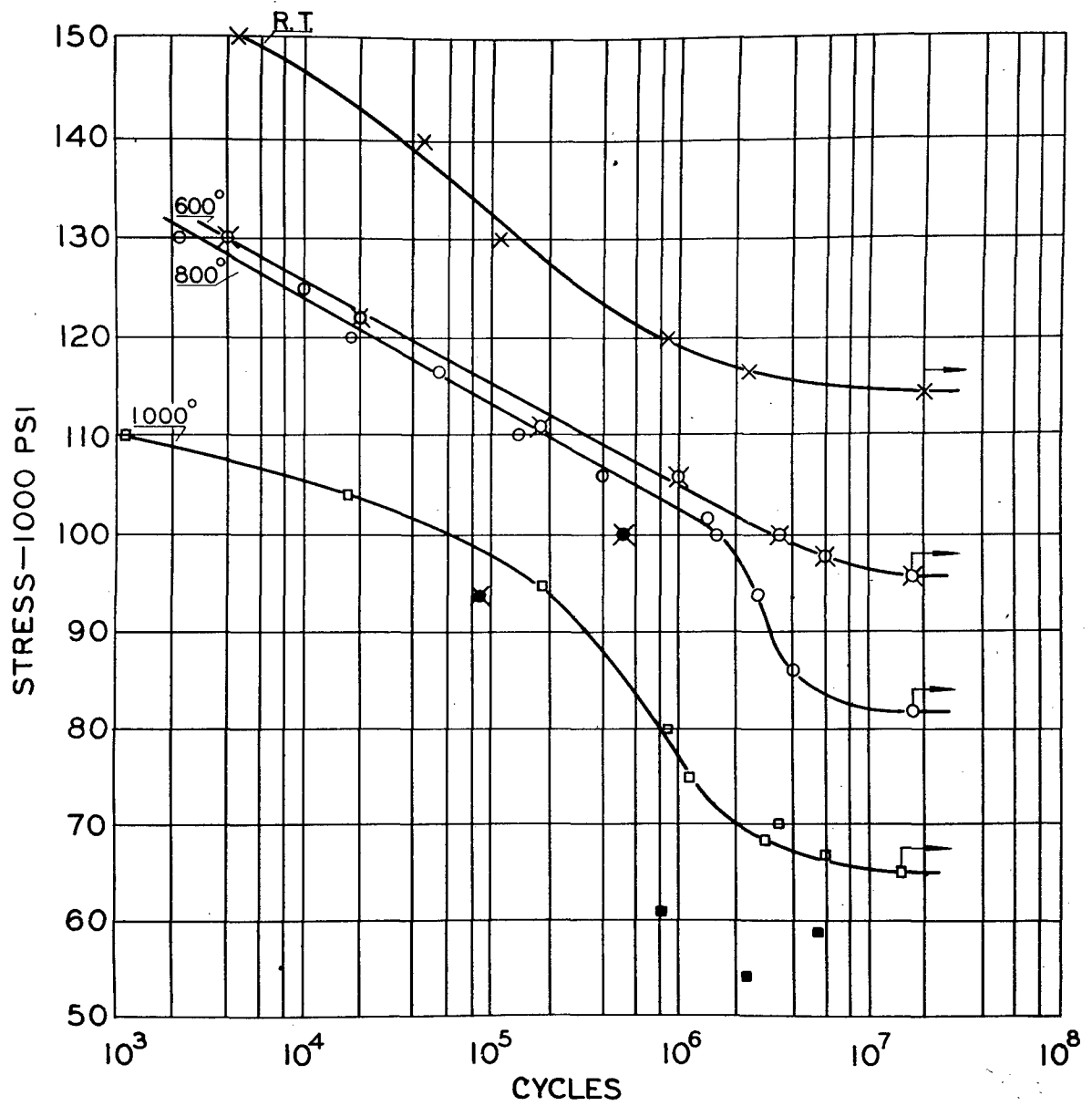
X ■ indicate extraordinary large inclusions

FIG. 6. S-N DIAGRAMS, TENSION, ZERO TO MAXIMUM, FOR ROOM AND ELEVATED TEMPERATURES, UNNOTCHED
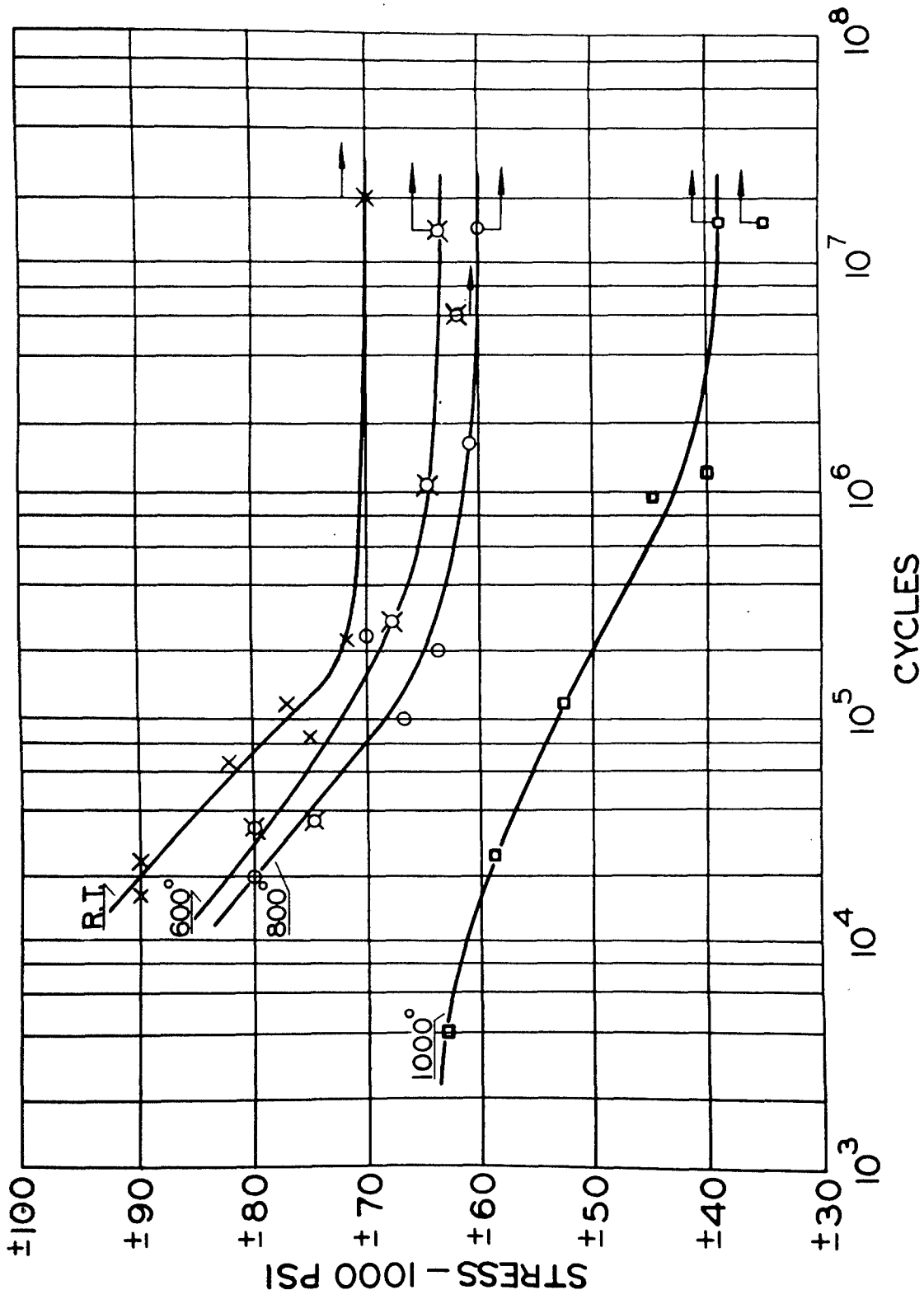
FIG. 7. S-N DIAGRAMS, COMPLETELY REVERSED, FOR ROOM AND ELEVATED TEMPERATURES, UNNOTCHED
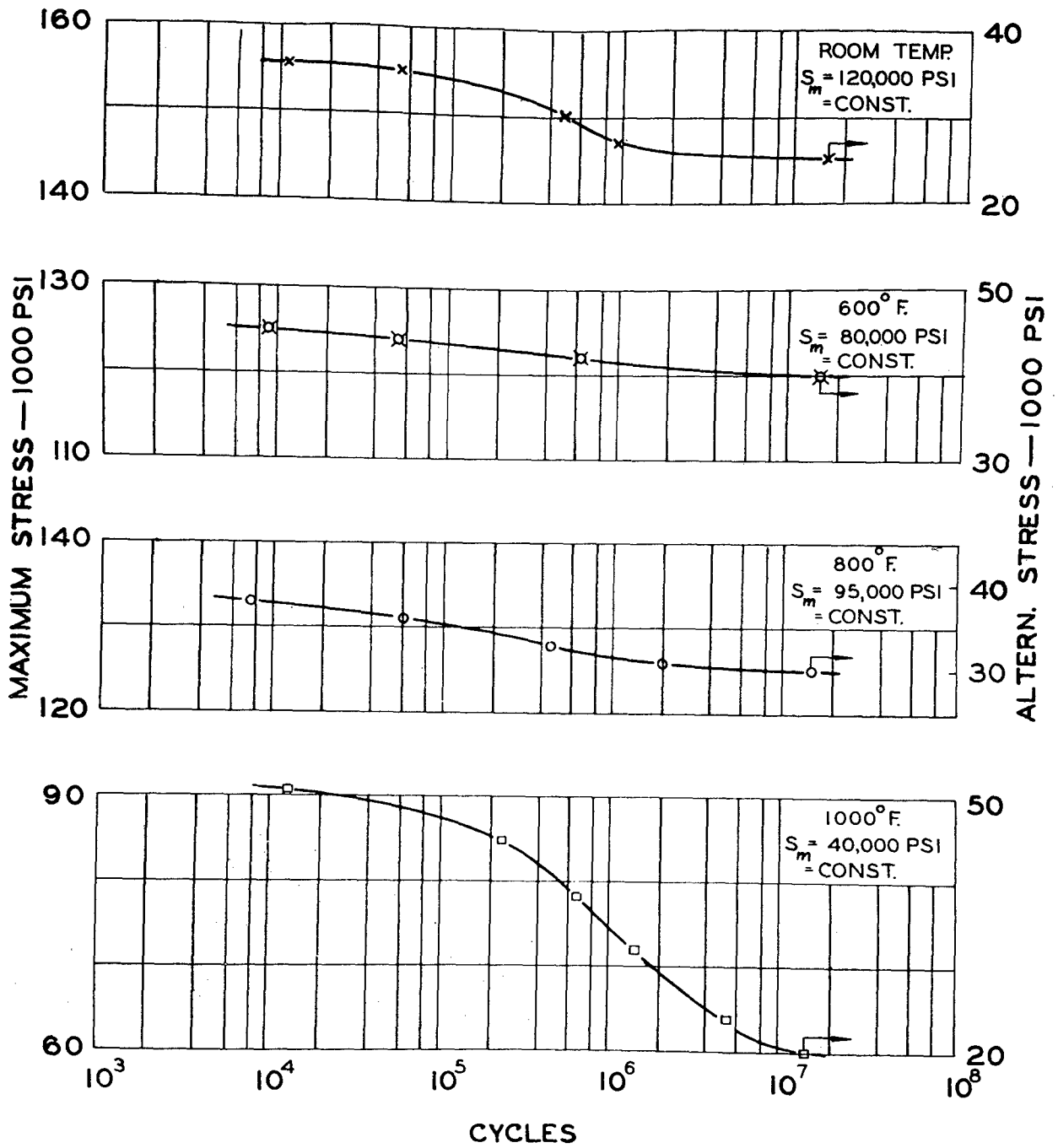
FIG. 8. S-N DIAGRAMS FOR HIGHER MEAN STRESSES, FOR ROOM AND ELEVATED TEMPERATURES, UNNOTCHED
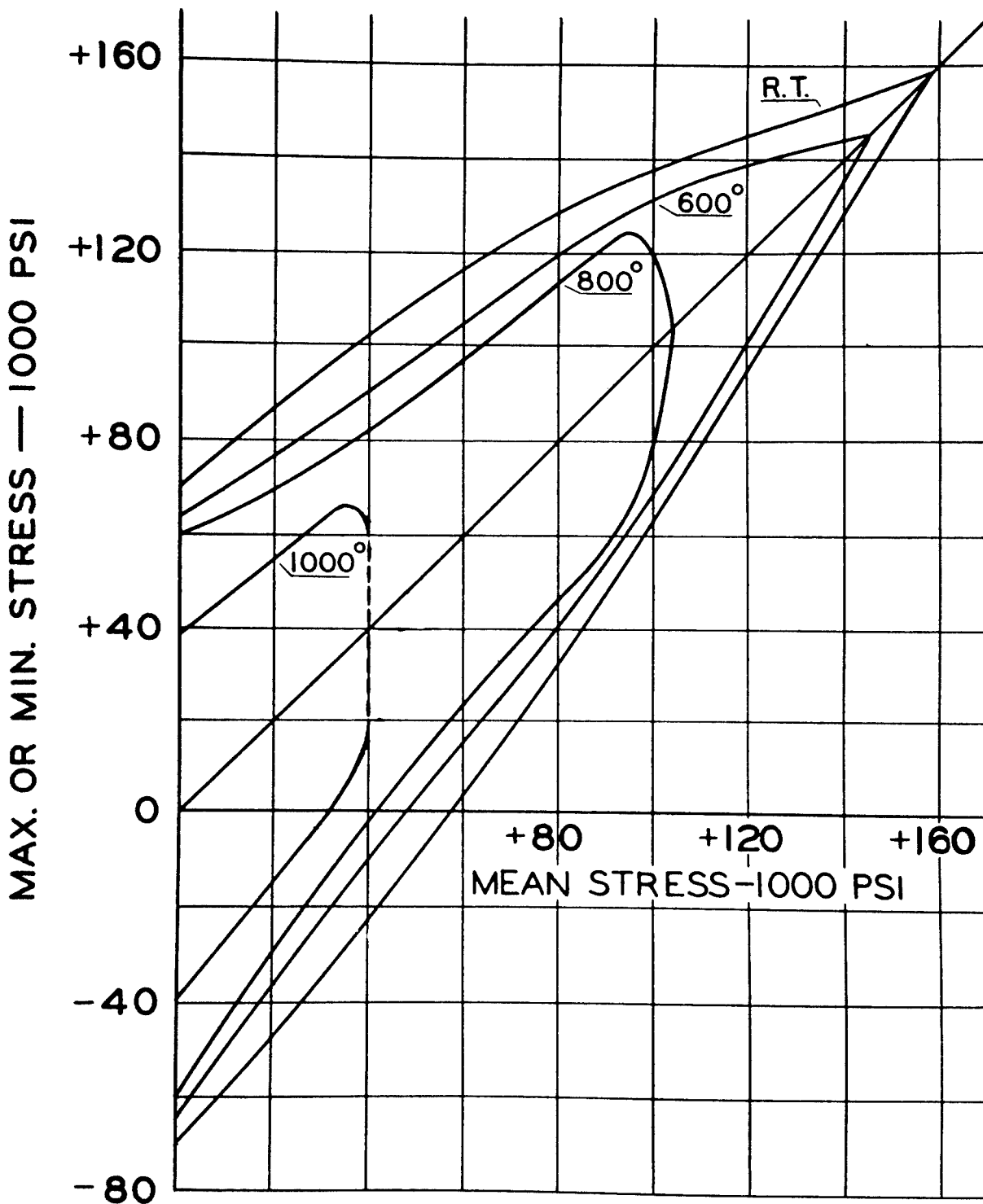
FIG. 9. MODIFIED GOODMAN DIAGRAMS, FOR ROOM AND ELEVATED TEMPERATURES, UNNOTCHED, AT 15×10^6 CYCLES
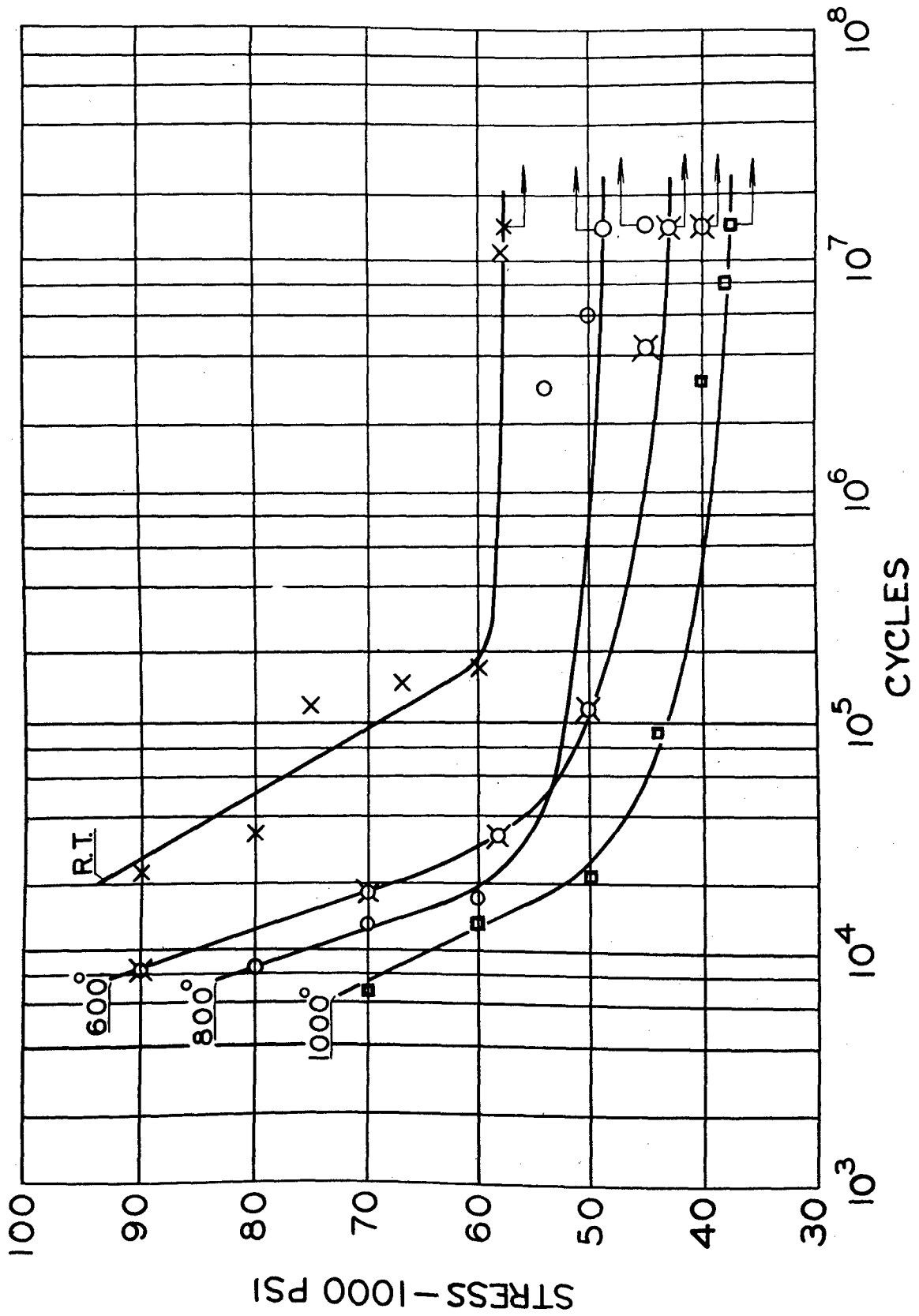
FIG. 10. S-N DIAGRAMS, TENSION, ZERO TO MAXIMUM, FOR ROOM AND ELEVATED TEMPERATURES, NOTCHED
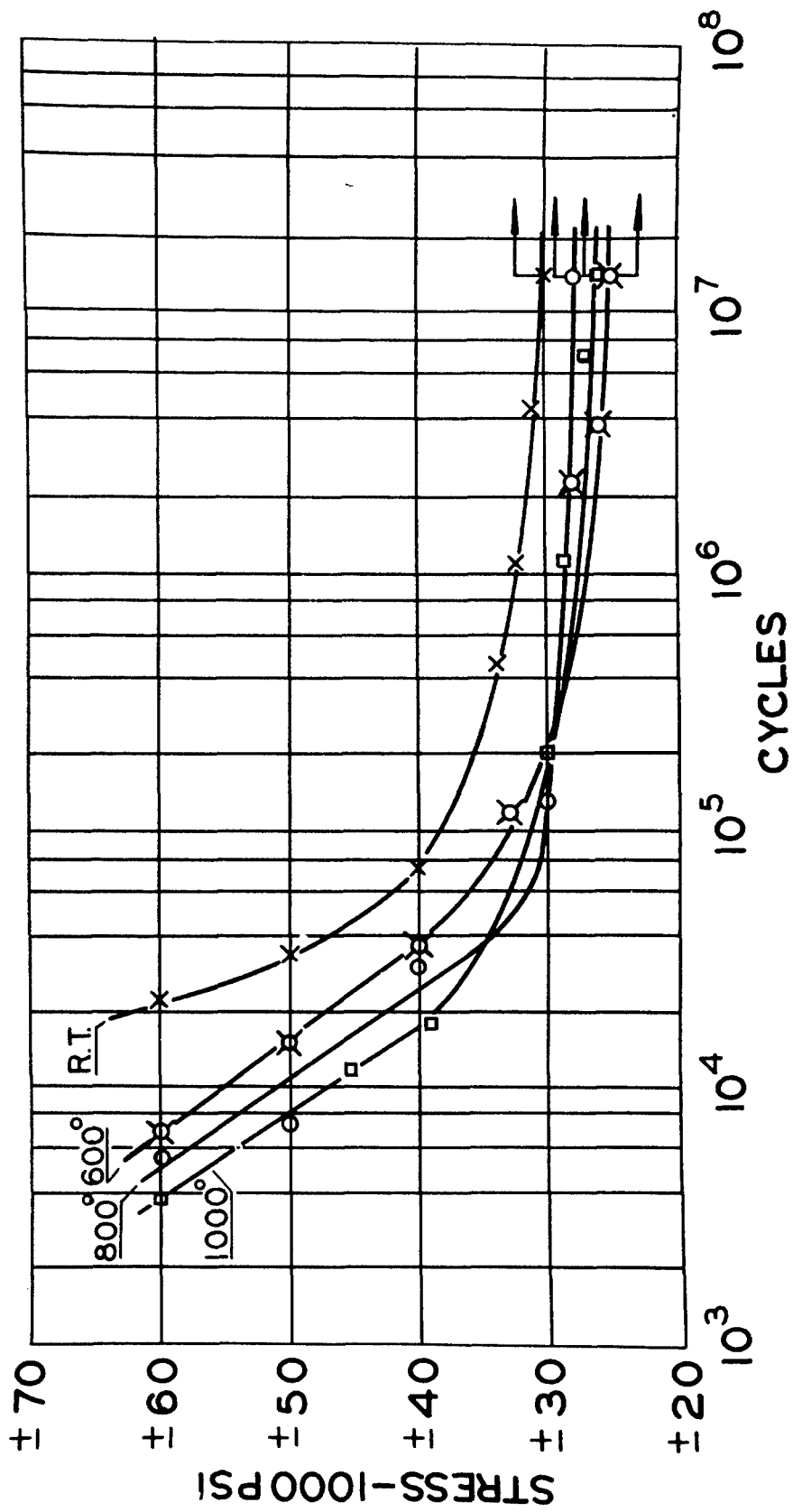
FIG. 11. S-N DIAGRAMS, COMPLETELY REVERSED, FOR ROOM AND ELEVATED TEMPERATURES, NOTCHED
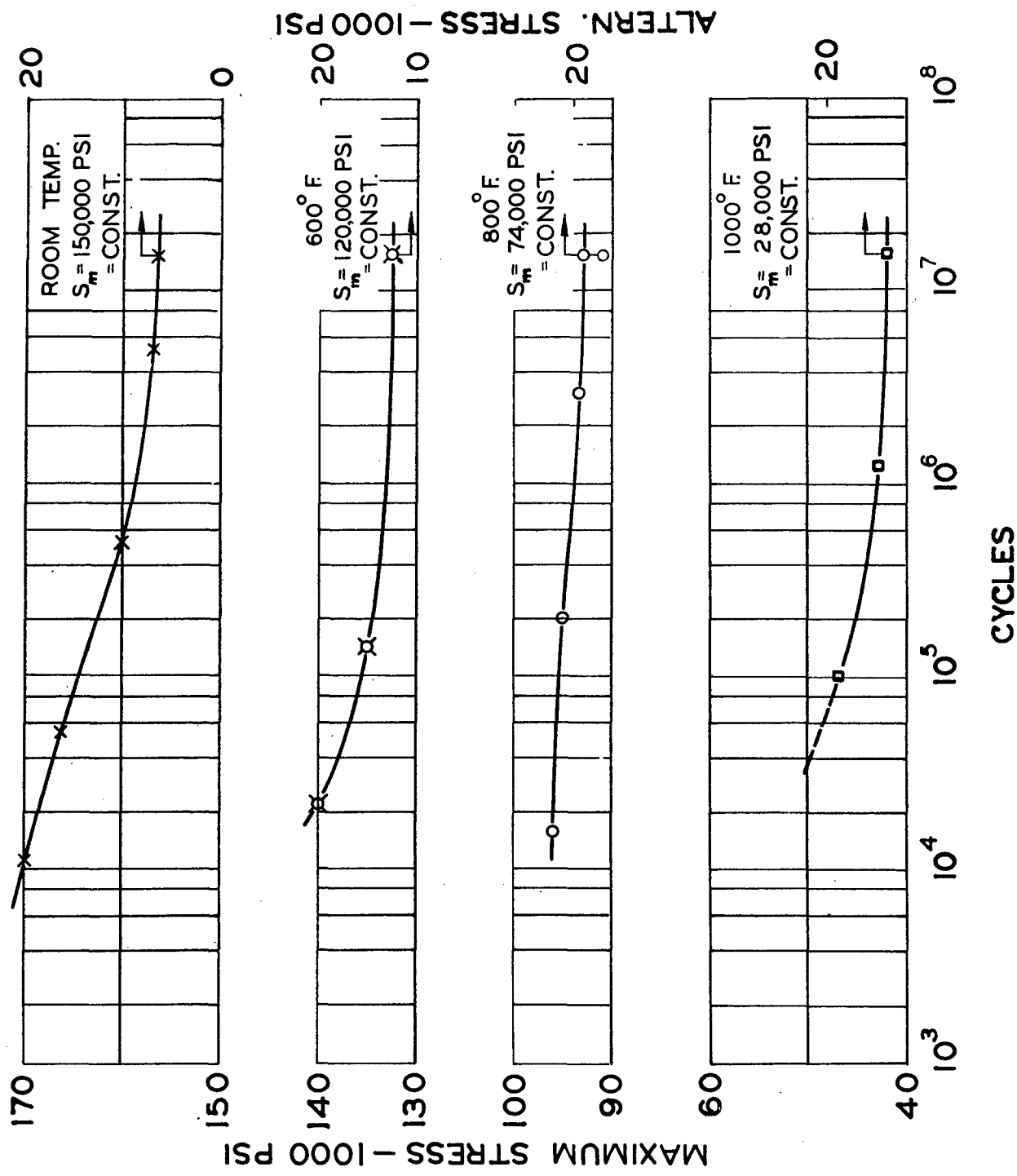
FIG. 12. S-N DIAGRAMS FOR HIGHER MEAN STRESSES, FOR ROOM AND ELEVATED TEMPERATURES, NOTCHED
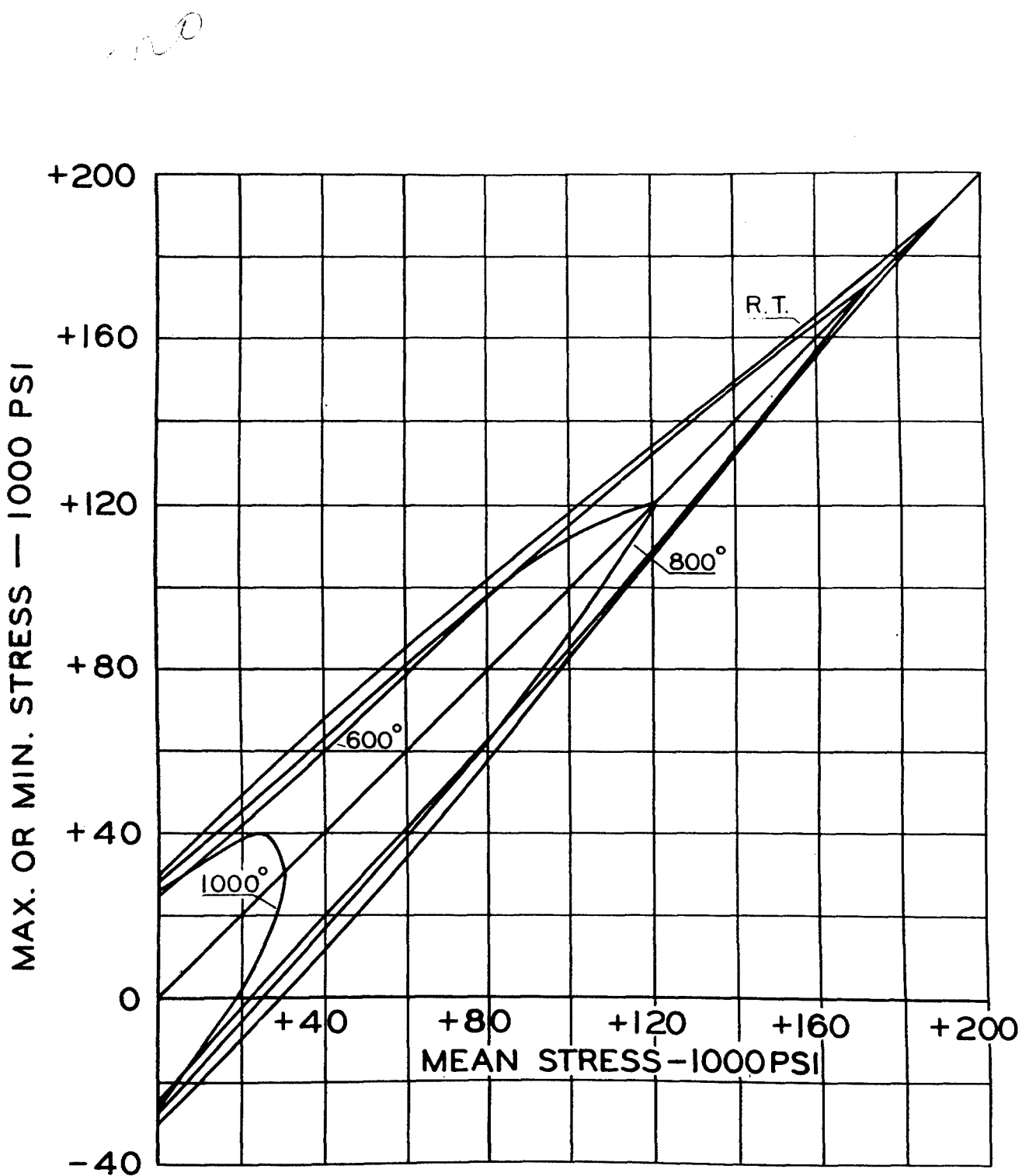
FIG. 13. MODIFIED GOODMAN DIAGRAMS, FOR ROOM AND ELEVATED TEMPERATURES, NOTCHED, AT 15×10^6 CYCLES
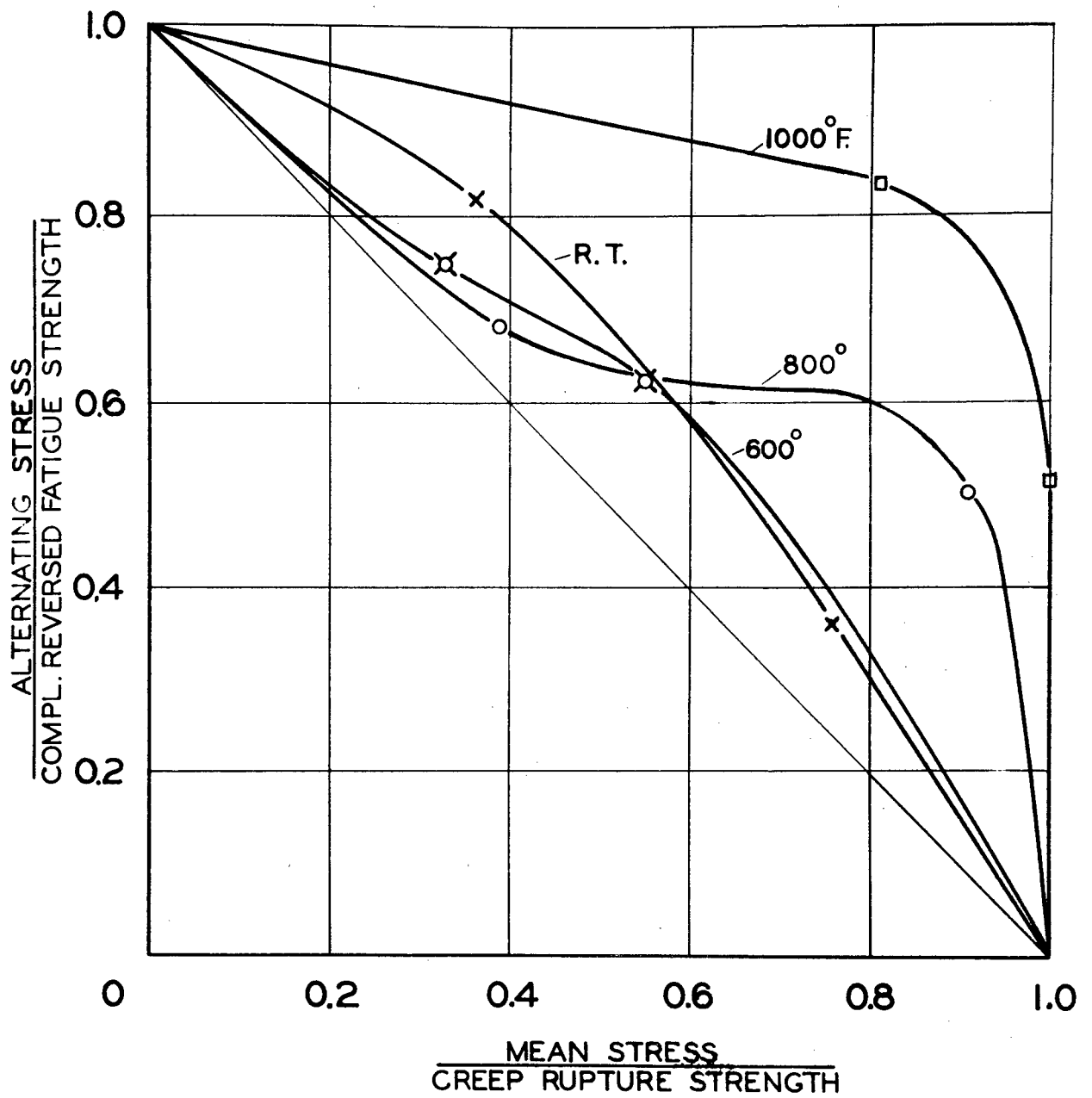
FIG. 14. NONDIMENSIONAL MODIFIED GOODMAN DIAGRAMS FOR ROOM AND ELEVATED TEMPERATURES, UNNOTCHED, AT 15 x 10^6 CYCLES
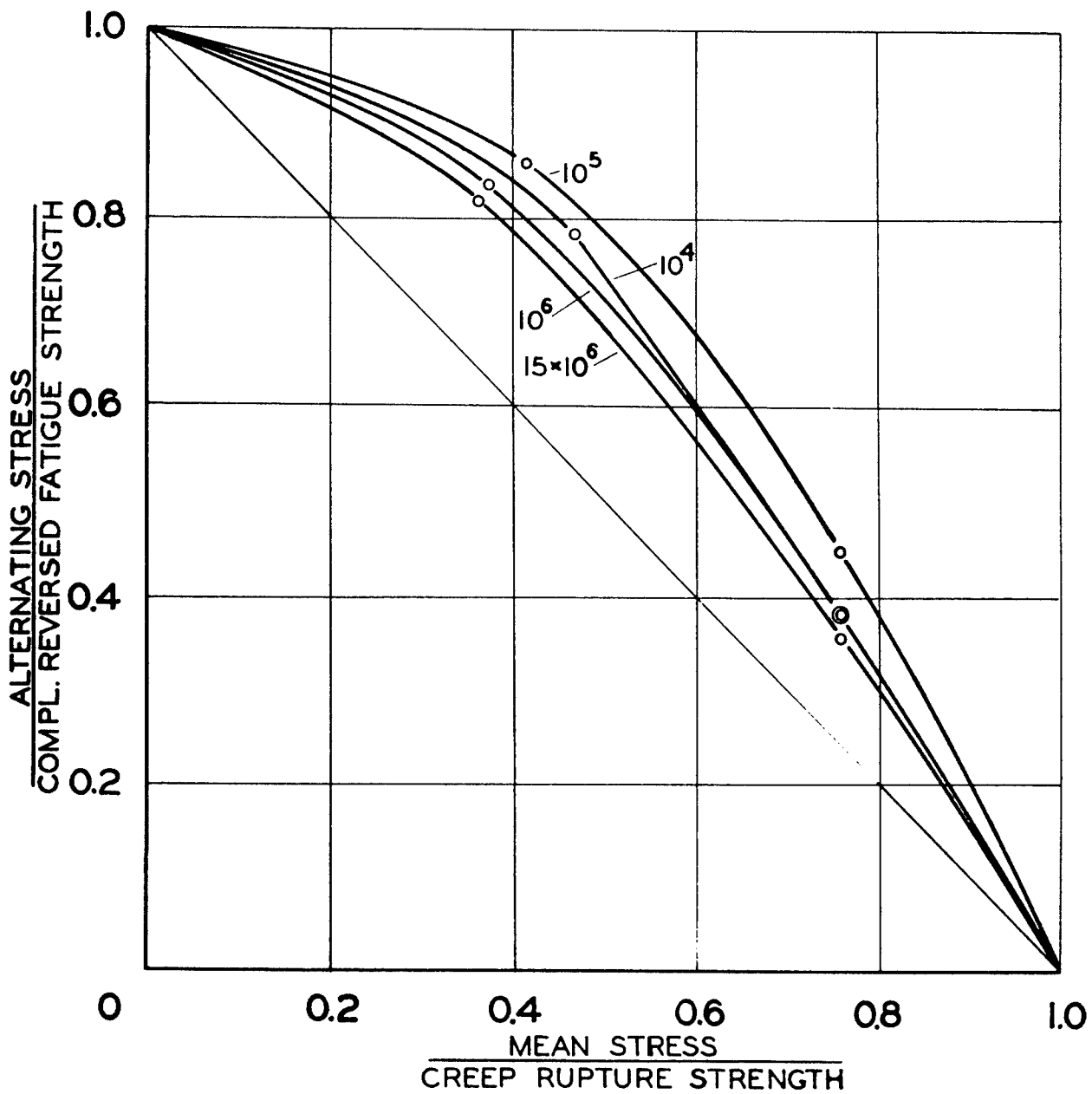
FIG. 15. NONDIMENSIONAL MODIFIED GOODMAN DIAGRAMS FOR DIFFERENT
LIFETIMES, AT ROOM TEMPERATURE, UNNOTCHED
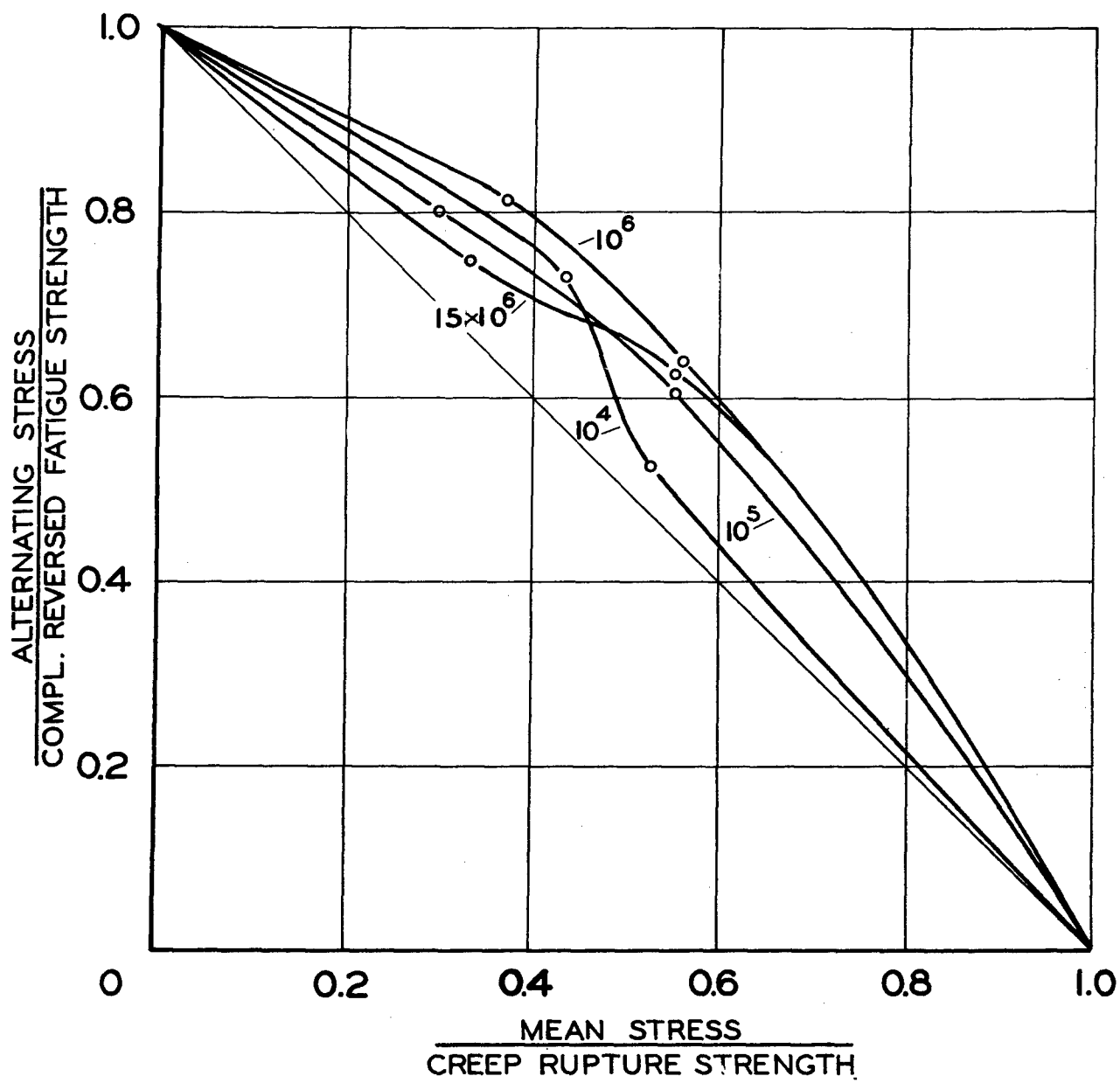
FIG. 16. NONDIMENSIONAL MODIFIED GOODMAN DIAGRAMS FOR DIFFERENT
LIFETIMES, AT 600° F., UNNOTCHED
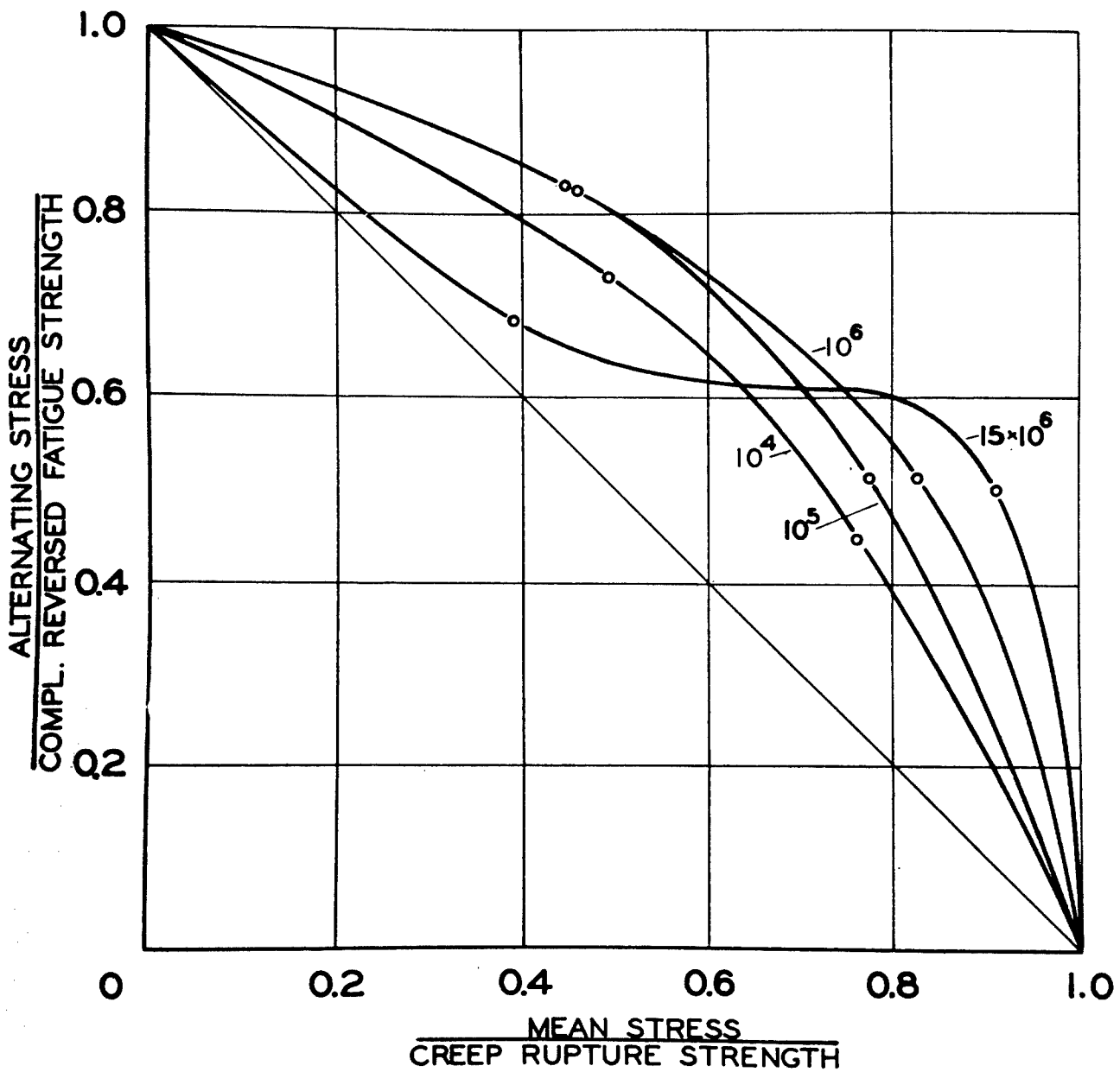
FIG. 17. NONDIMENSIONAL MODIFIED GOODMAN DIAGRAMS FOR DIFFERENT
LIFETIMES, AT 800° F., UNNOTCHED
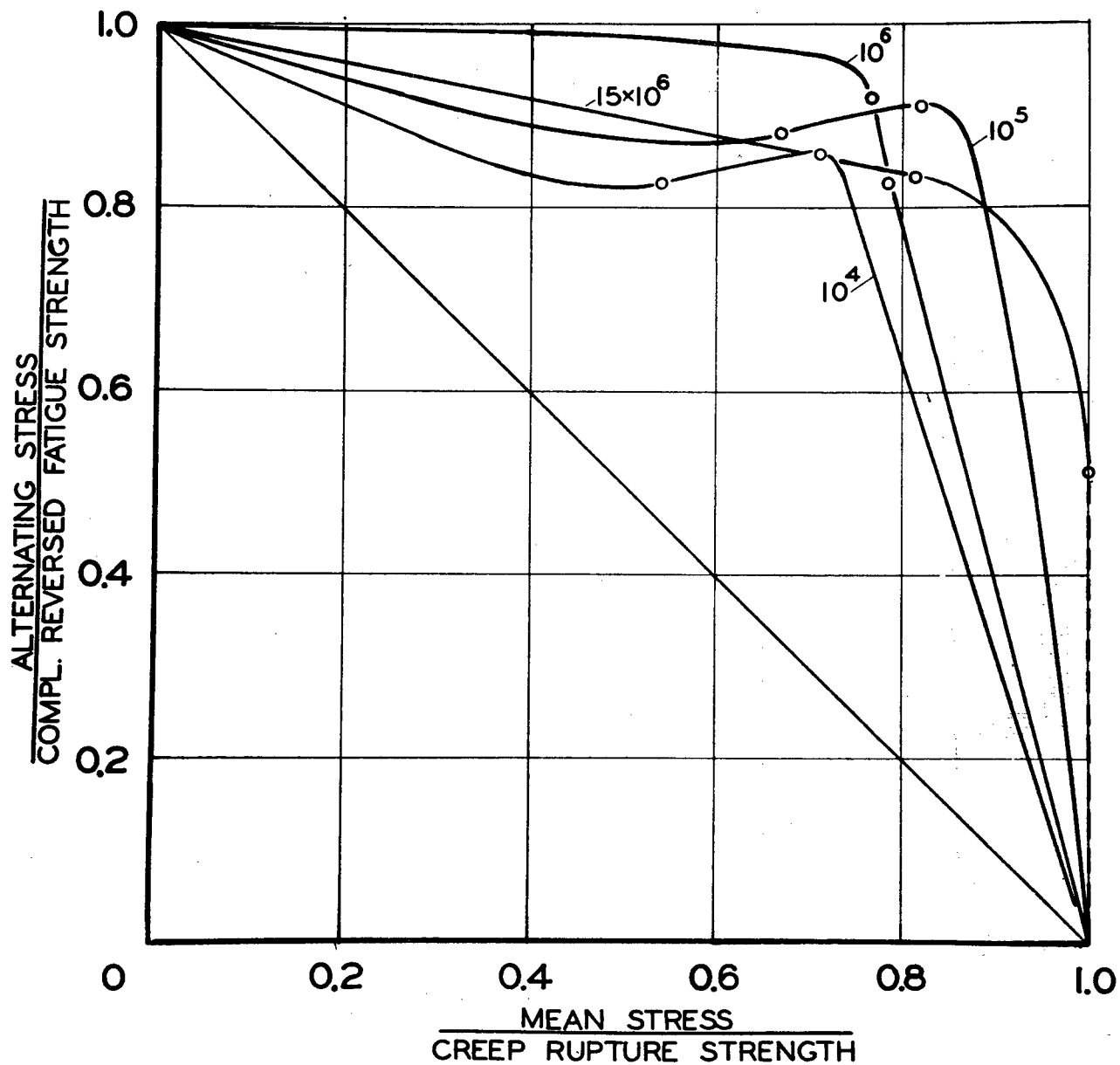
FIG. 18. NONDIMENSIONAL MODIFIED GOODMAN DIAGRAMS FOR DIFFERENT
LIFETIMES, AT 1000° F., UNNOTCHED
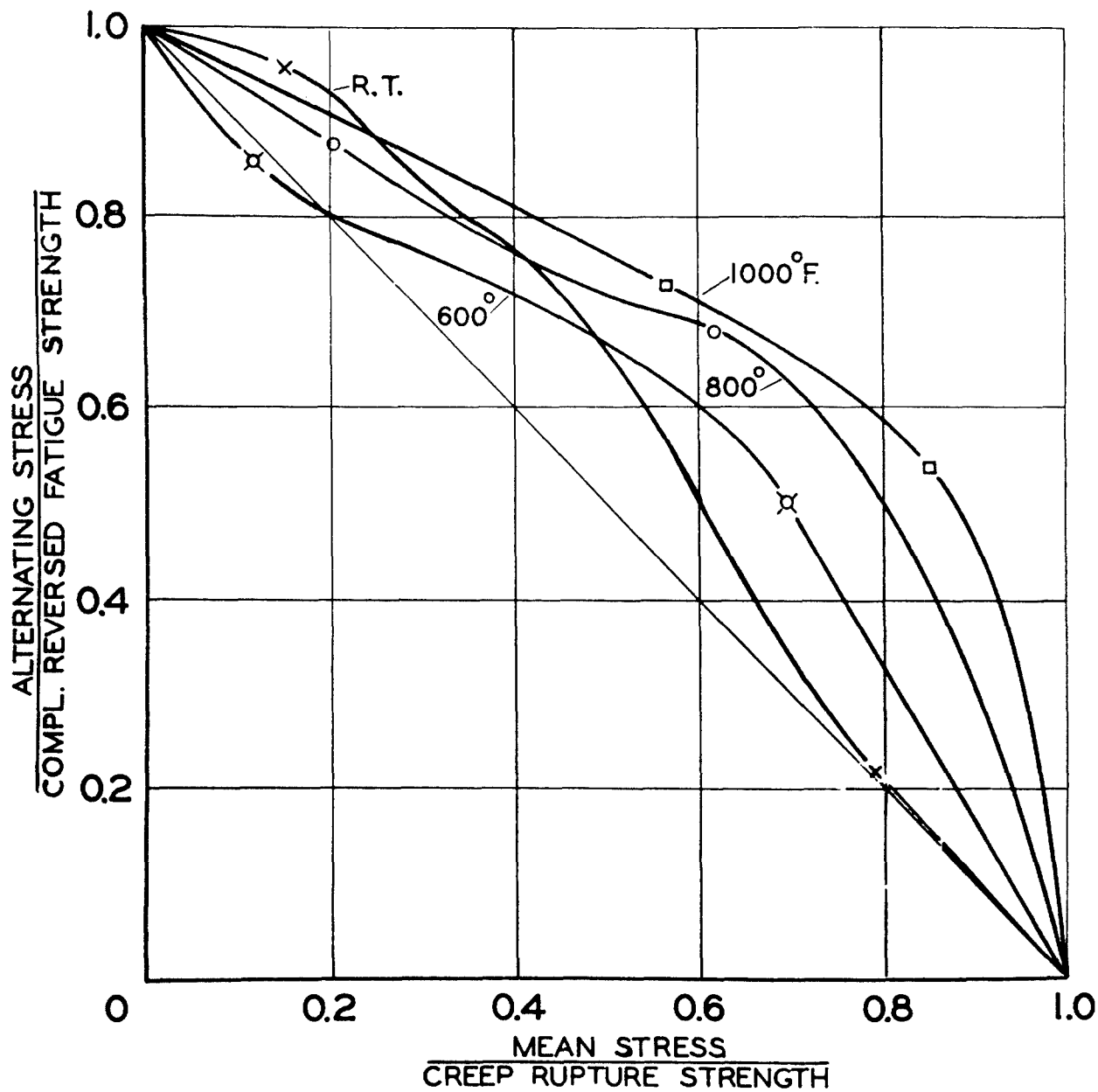
FIG. 19. NONDIMENSIONAL MODIFIED GOODMAN DIAGRAMS FOR ROOM AND
ELEVATED TEMPERATURES, NOTCHED, AT 15×10^6 CYCLES
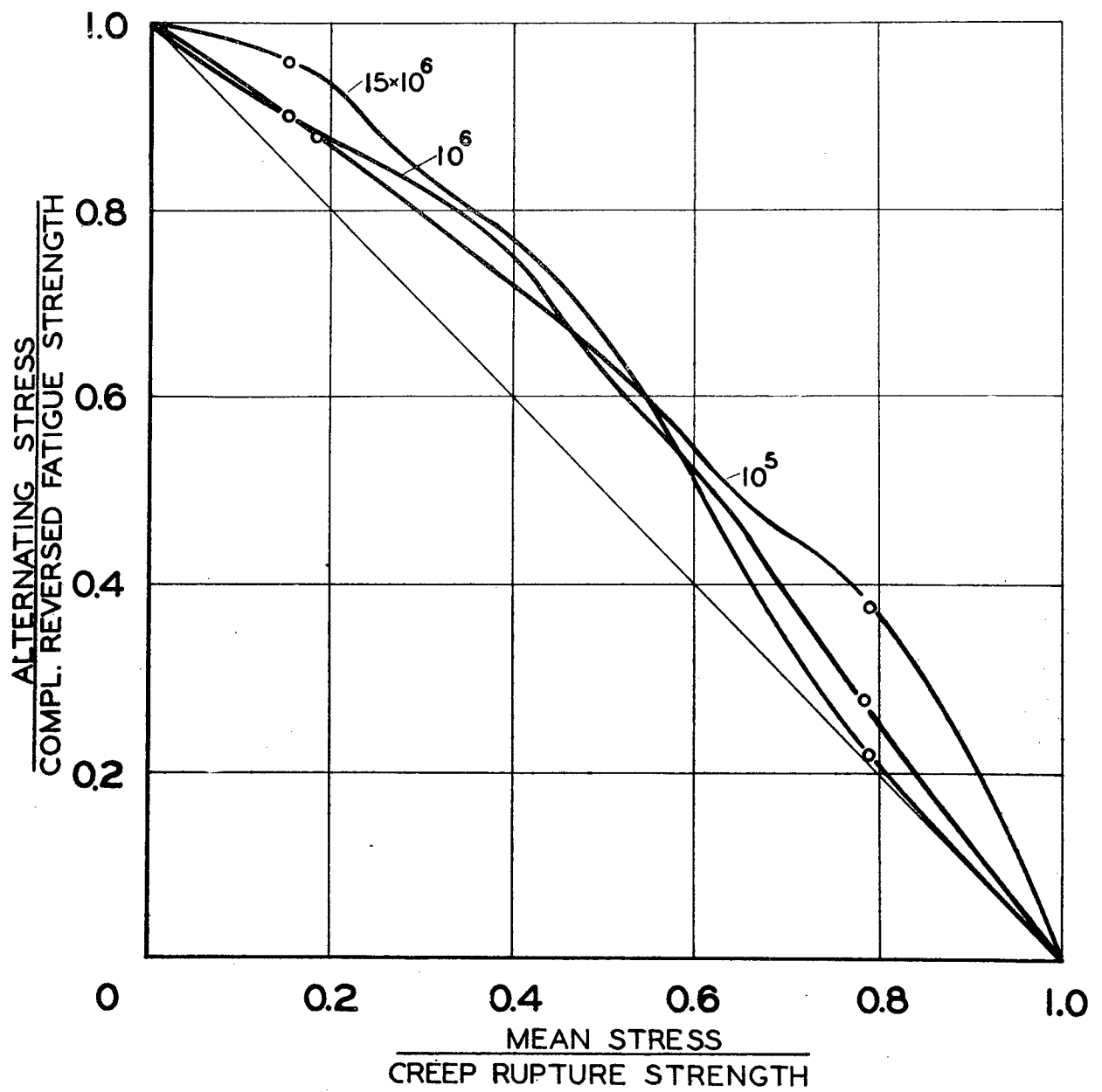
FIG. 20.   NONDIMENSIONAL MODIFIED GOODMAN DIAGRAMS FOR DIFFERENT
LIFETIMES, AT ROOM TEMPERATURE, NOTCHED
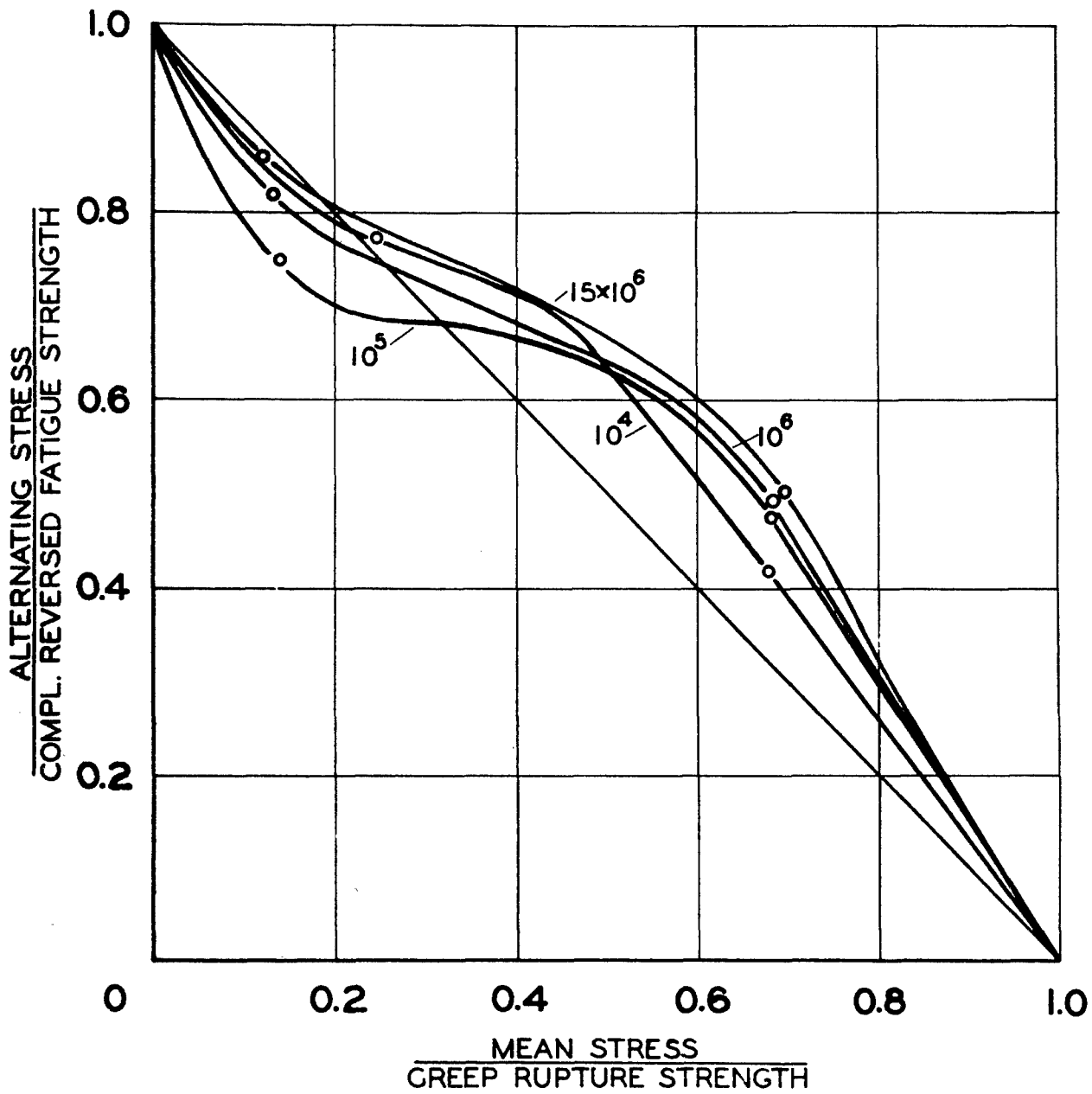
FIG. 21. NONDIMENSIONAL MODIFIED GOODMAN DIAGRAMS FOR DIFFERENT LIFETIMES, AT 600° F., NOTCHED
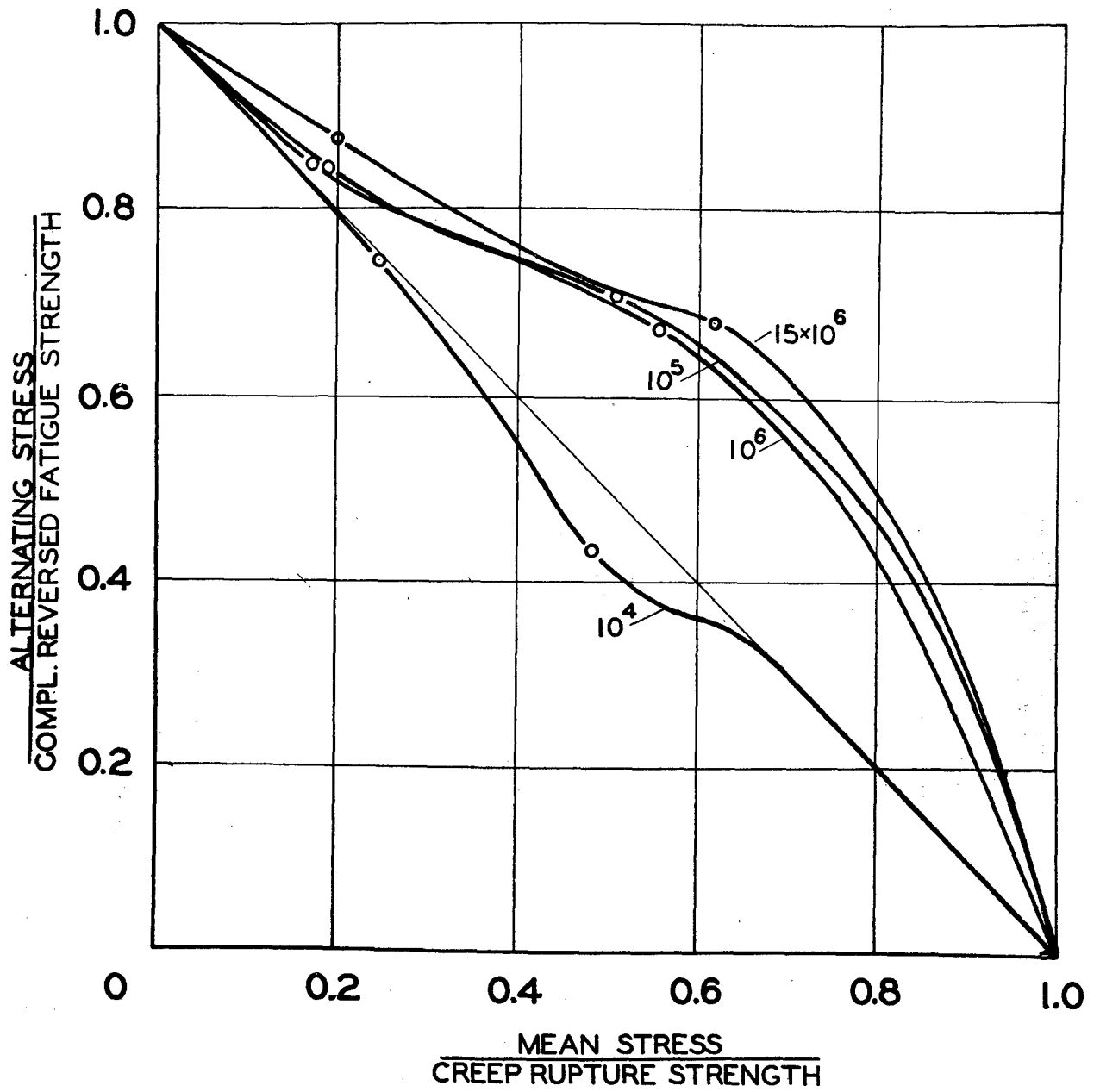
FIG. 22. NONDIMENSIONAL MODIFIED GOODMAN DIAGRAMS FOR DIFFERENT LIFETIMES, AT 800° F., NOTCHED
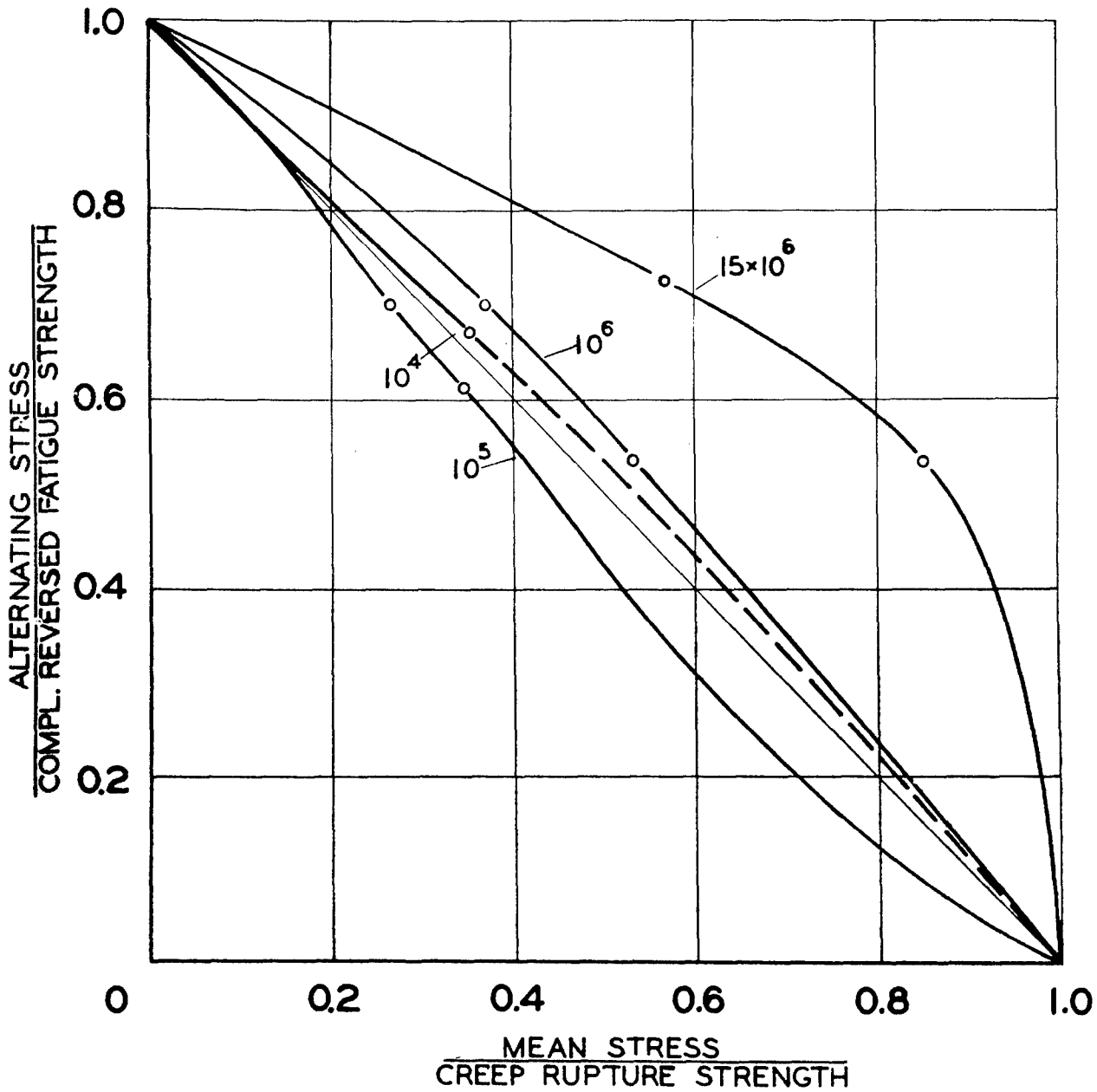
FIG. 23. NONDIMENSIONAL MODIFIED GOODMAN DIAGRAMS FOR DIFFERENT
LIFETIMES, AT 1000° F., NOTCHED
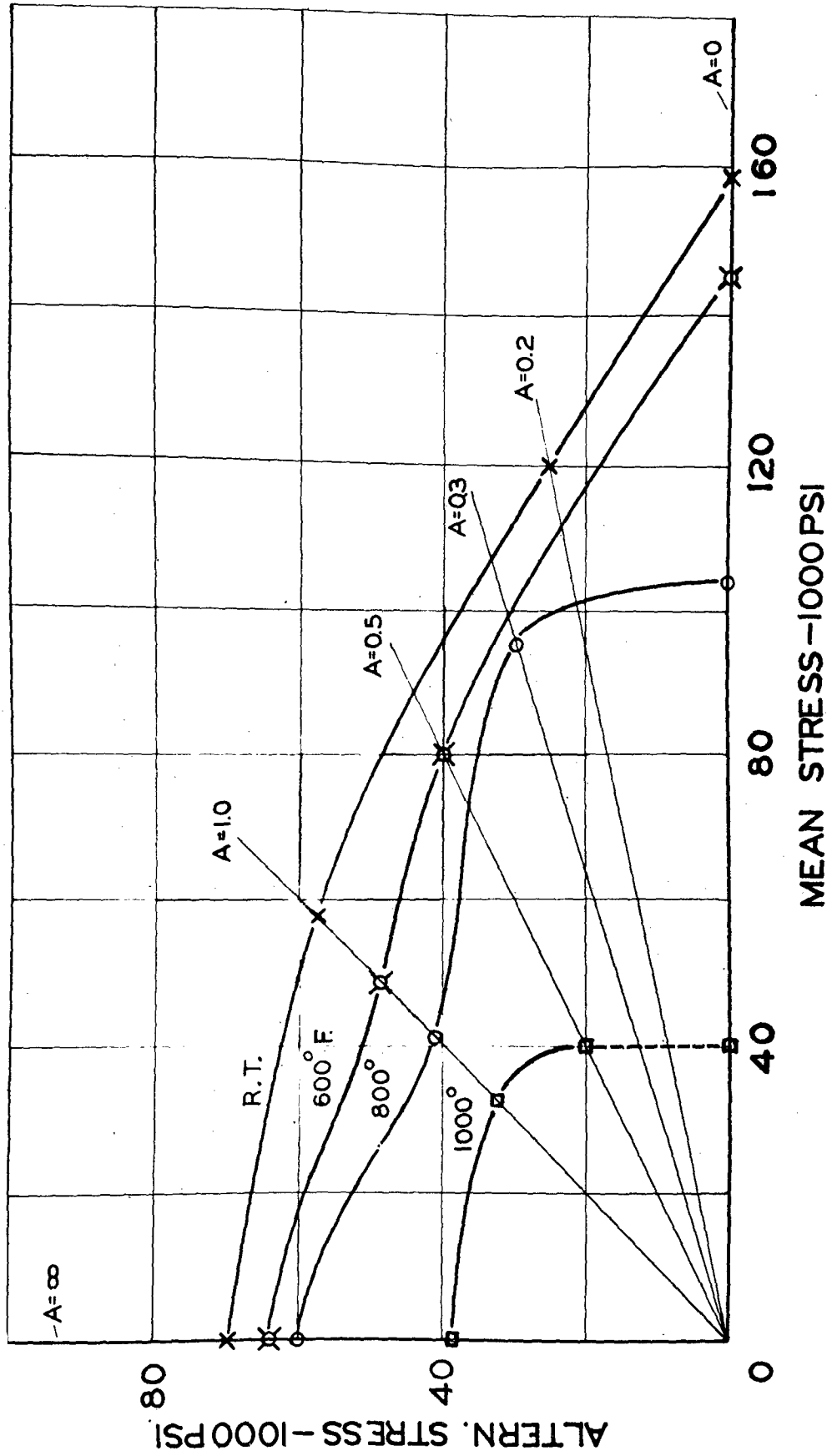
FIG. 24. ALTERNATING STRESS - MEAN STRESS DIAGRAMS. FOR ROOM AND ELEVATED TEMPERATURES, UNNOTCHED, AT 15 x 10⁶ CYCLES
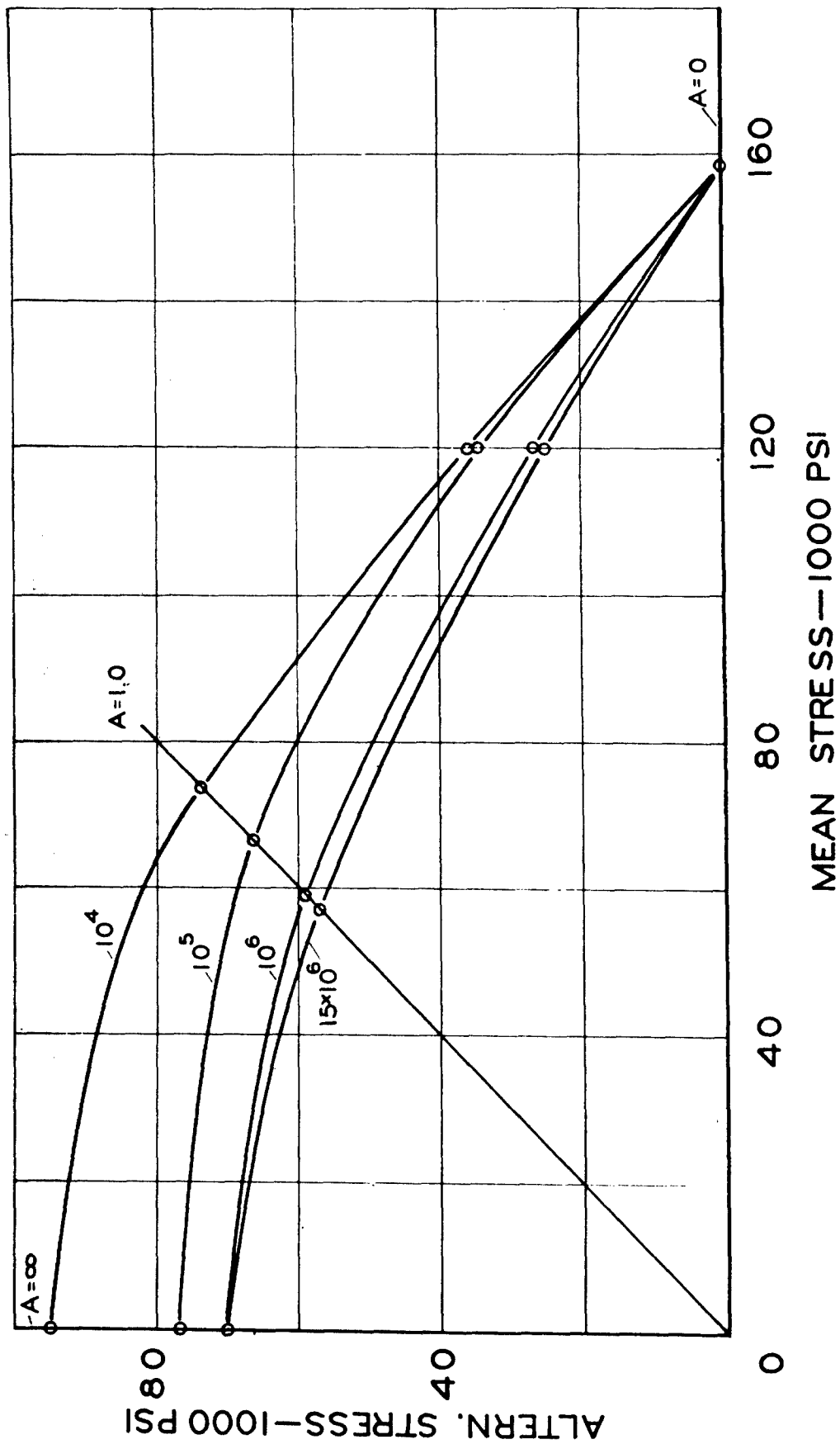
FIG. 25. ALTERNATING STRESS - MEAN STRESS DIAGRAMS FOR DIFFERENT LIFETIMES, AT ROOM TEMPERATURE, UNNOTCHED
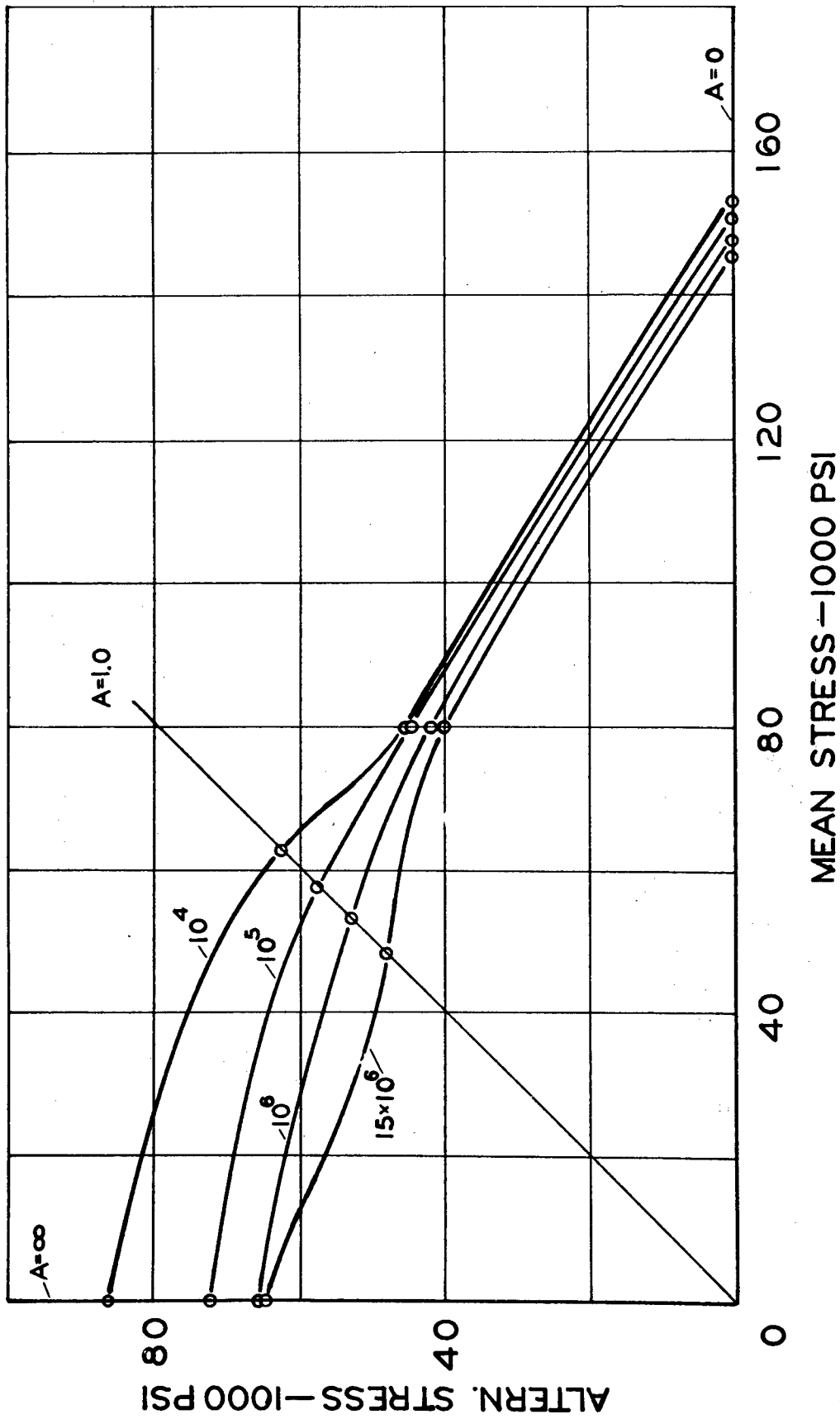
FIG. 26. ALTERNATING STRESS - MEAN STRESS DIAGRAMS FOR DIFFERENT LIFETIMES, AT 600° F., UNNOTCHED
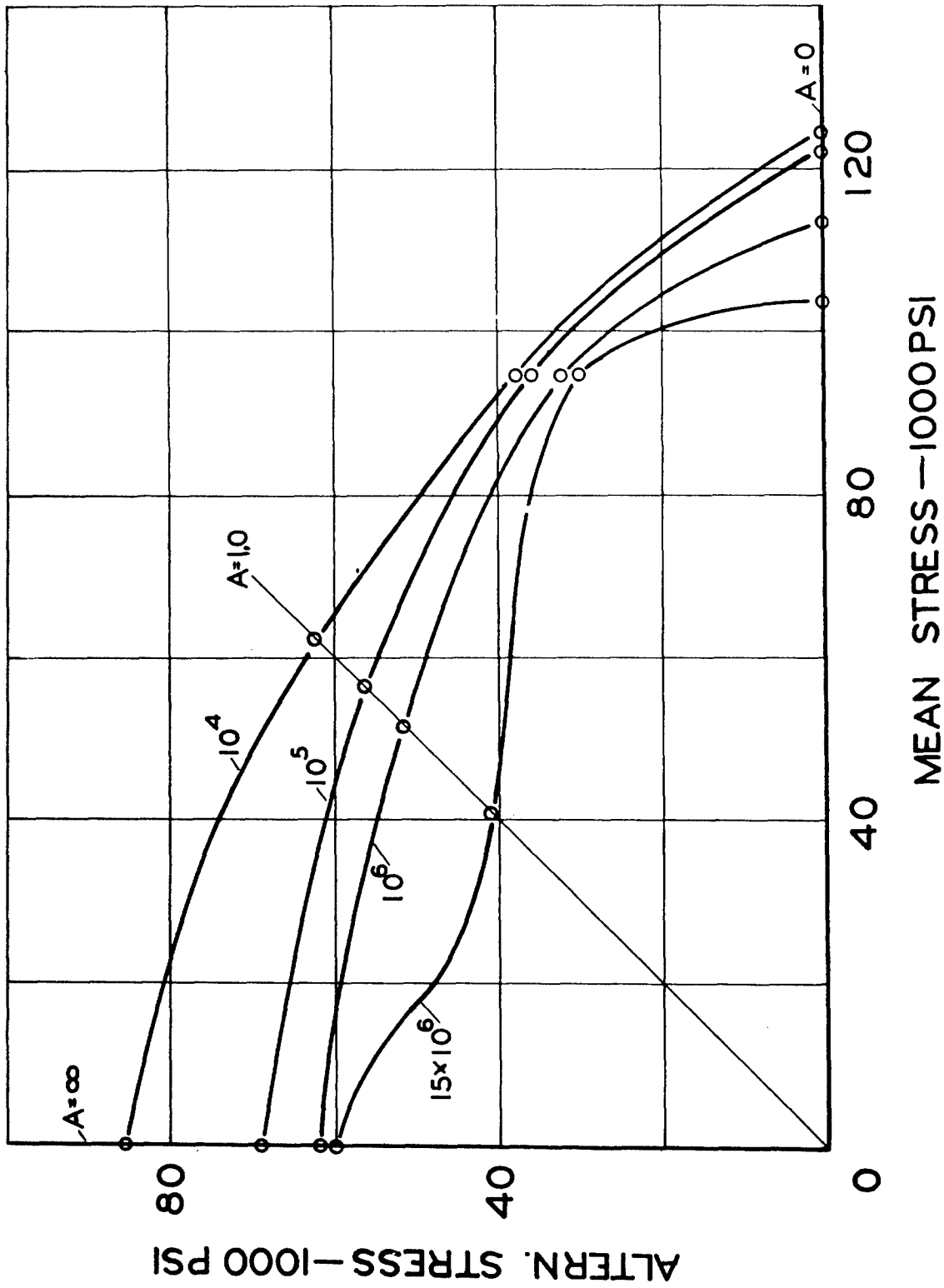
FIG. 27. ALTERNATING STRESS – MEAN STRESS DIAGRAMS FOR DIFFERENT LIFETIMES, AT 800° F., UNNOTCHED
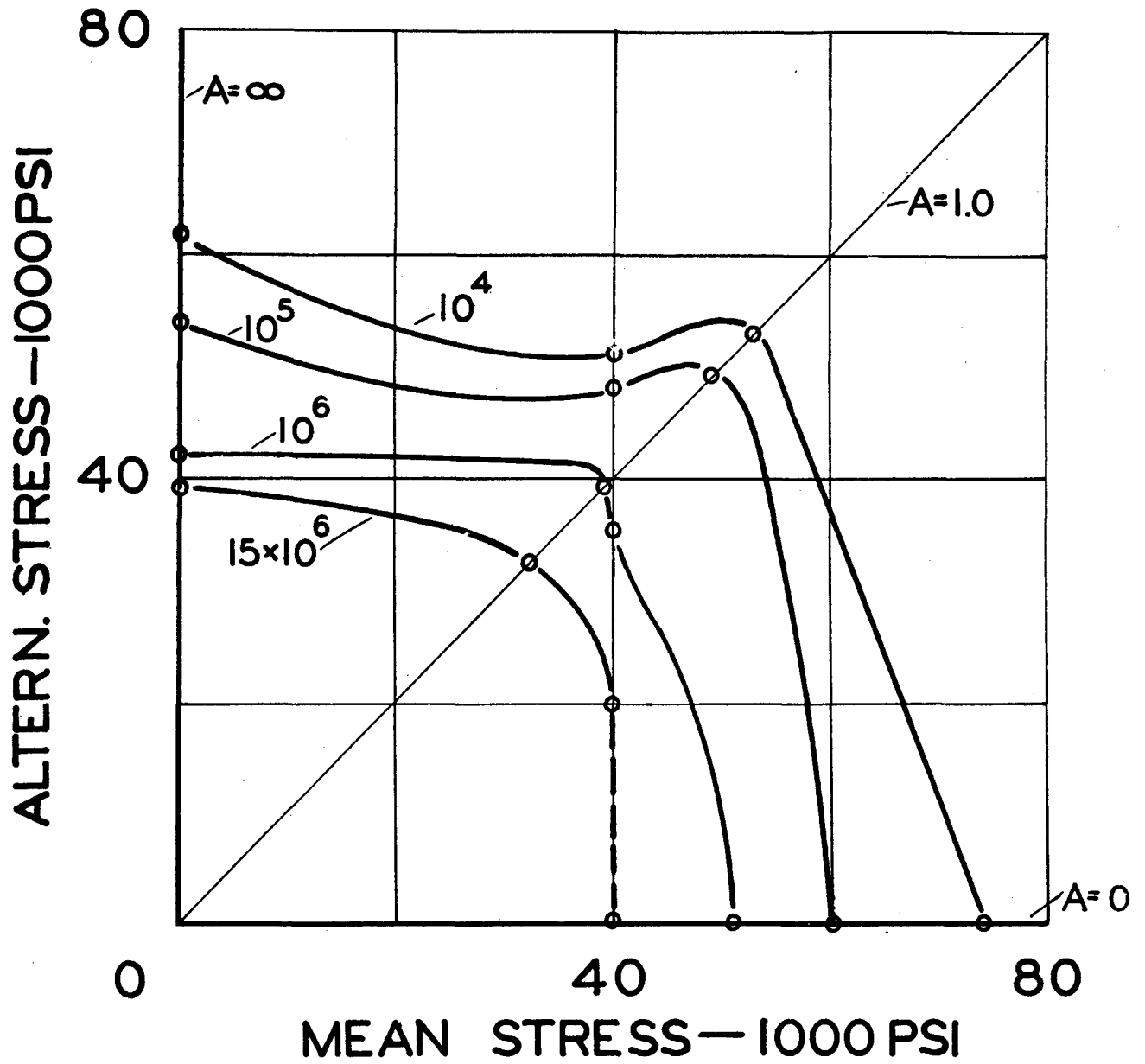
FIG. 28. ALTERNATING STRESS – MEAN STRESS DIAGRAMS FOR DIFFERENT LIFETIMES, AT 1000° F., UNNOTCHED
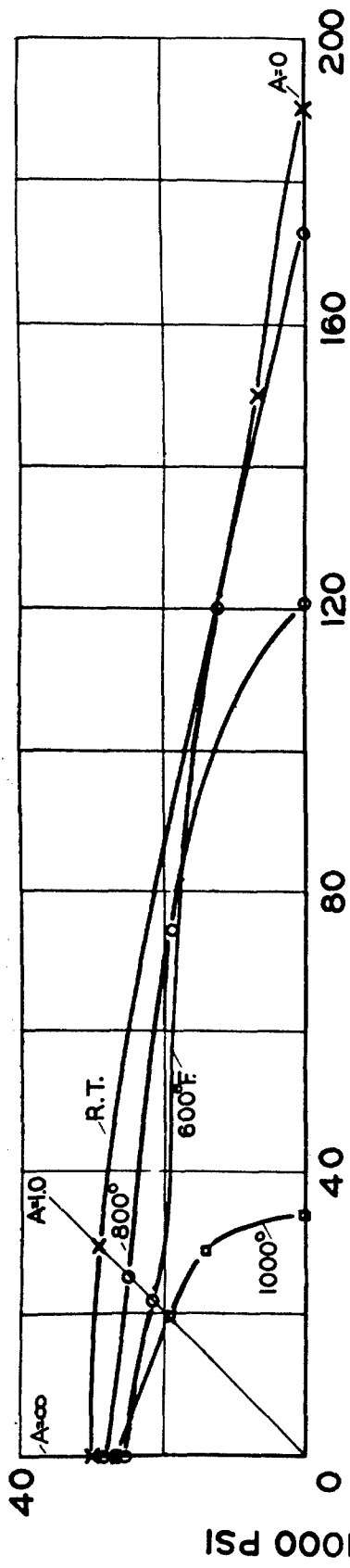
FIG. 29. ALTERNATING STRESS – MEAN STRESS DIAGRAMS FOR ROOM AND ELEVATED TEMPERATURES, NOTCHED, AT 15 x 10⁶ CYCLES

FIG. 30. ALTERNATING STRESS – MEAN STRESS DIAGRAMS FOR DIFFERENT LIFETIMES, AT ROOM TEMPERATURE, NOTCHED

MEAN STRESS—1000 PSI
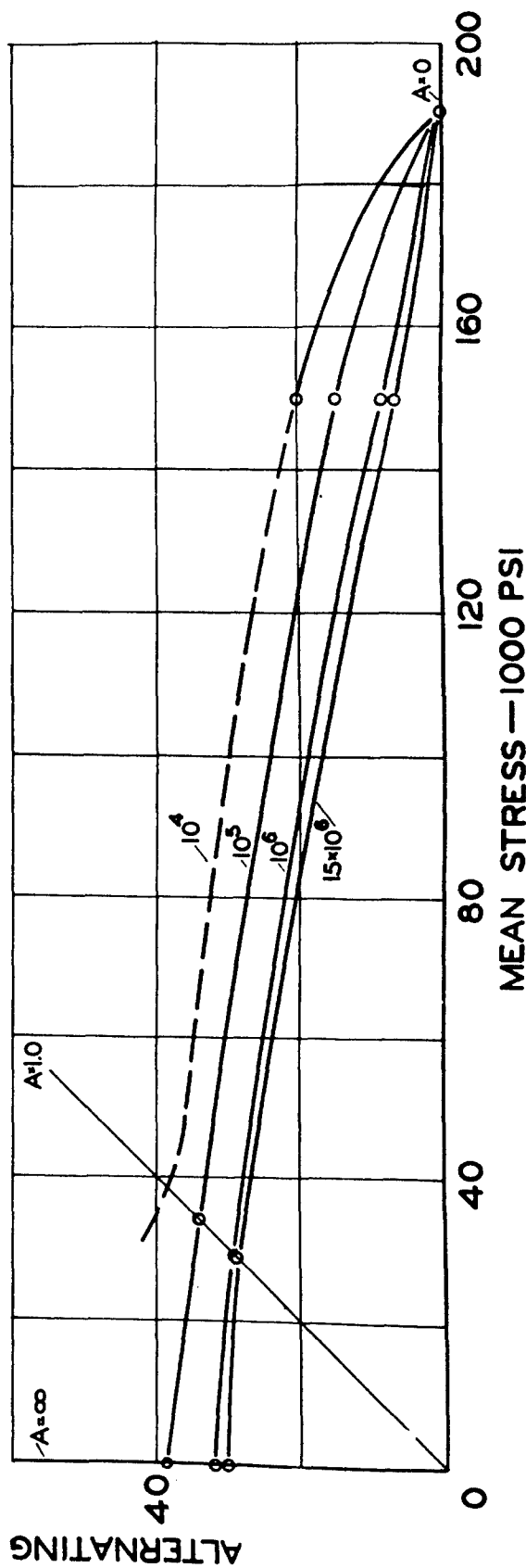
ALTERNATING STRESS—1000 PSI
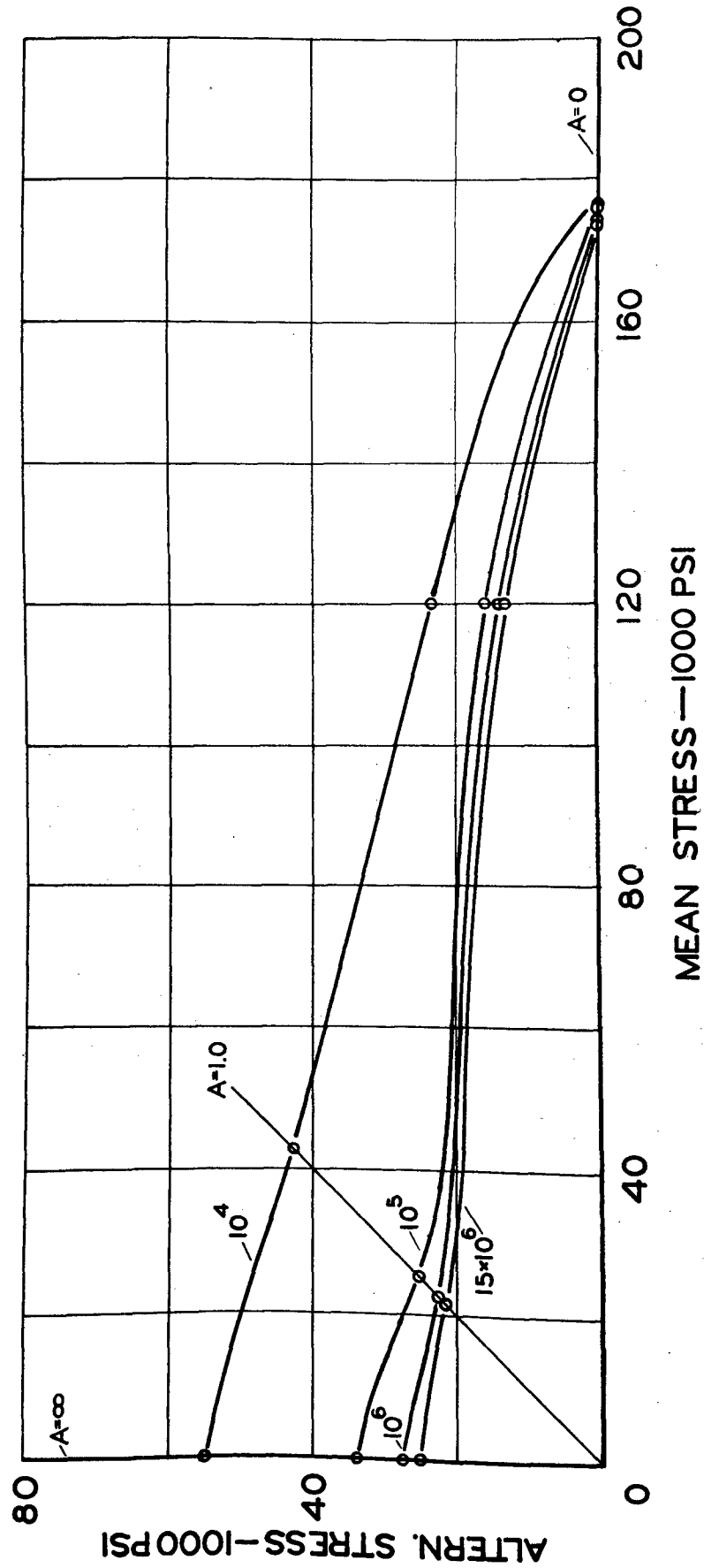
FIG. 31. ALTERNATING STRESS – MEAN STRESS DIAGRAMS FOR DIFFERENT LIFETIMES, AT 600° F., NOTCHED
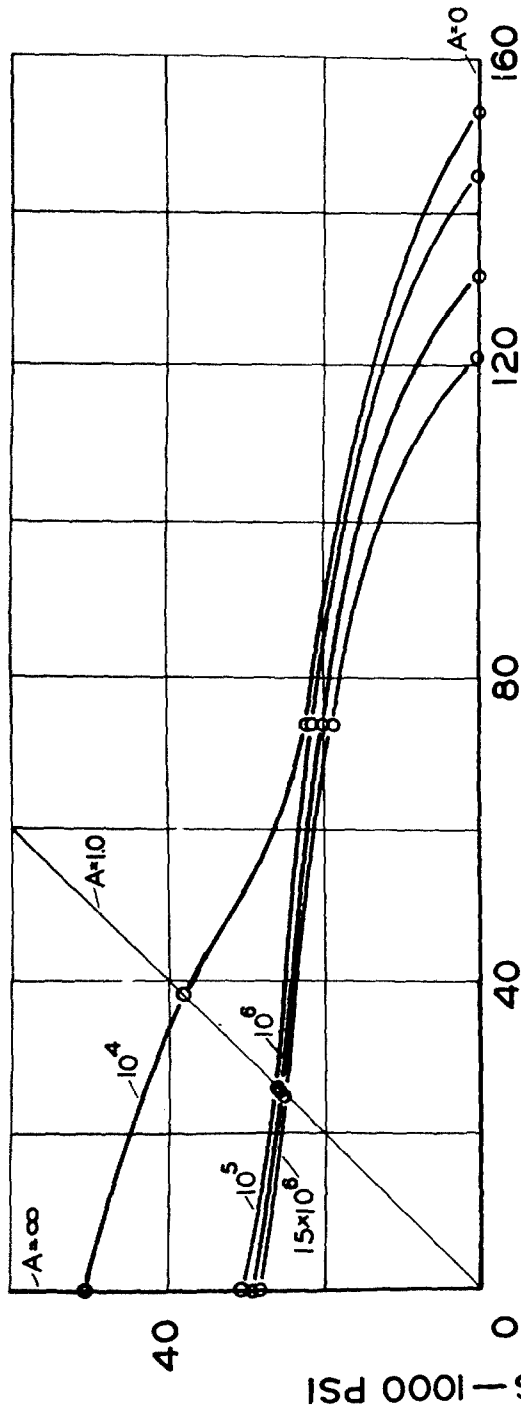
FIG. 32. ALTERNATING STRESS – MEAN STRESS DIAGRAMS FOR DIFFERENT LIFETIMES AT 800° F., NOTCHED
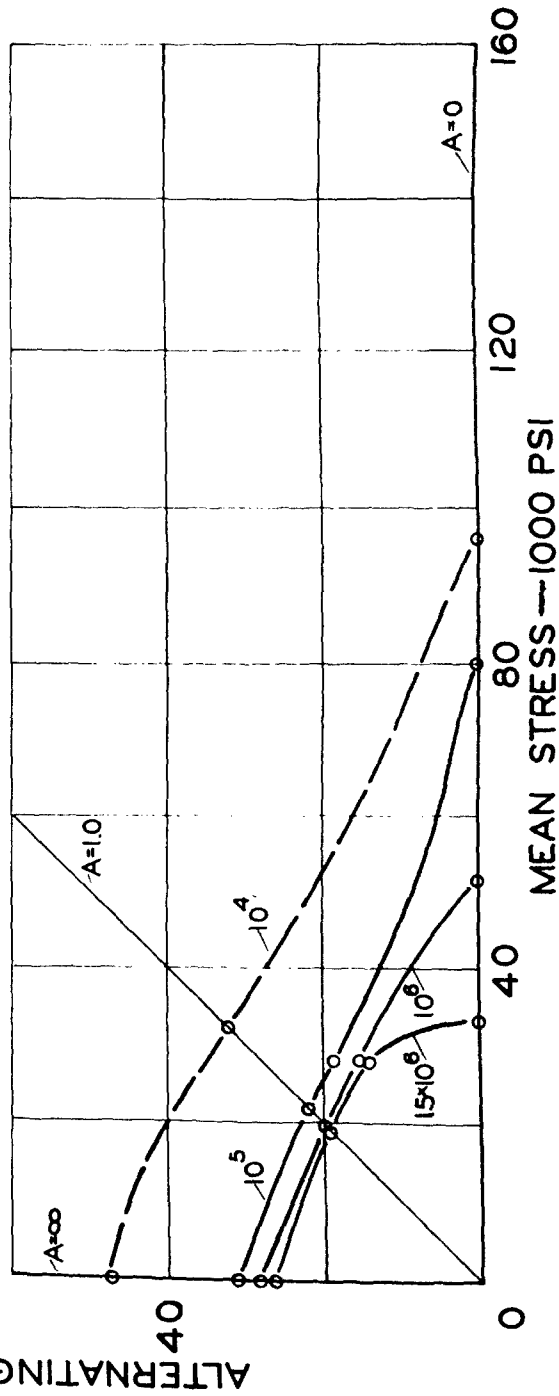
FIG. 33. ALTERNATING STRESS – MEAN STRESS DIAGRAMS FOR DIFFERENT LIFETIMES AT 1000° F., NOTCHED
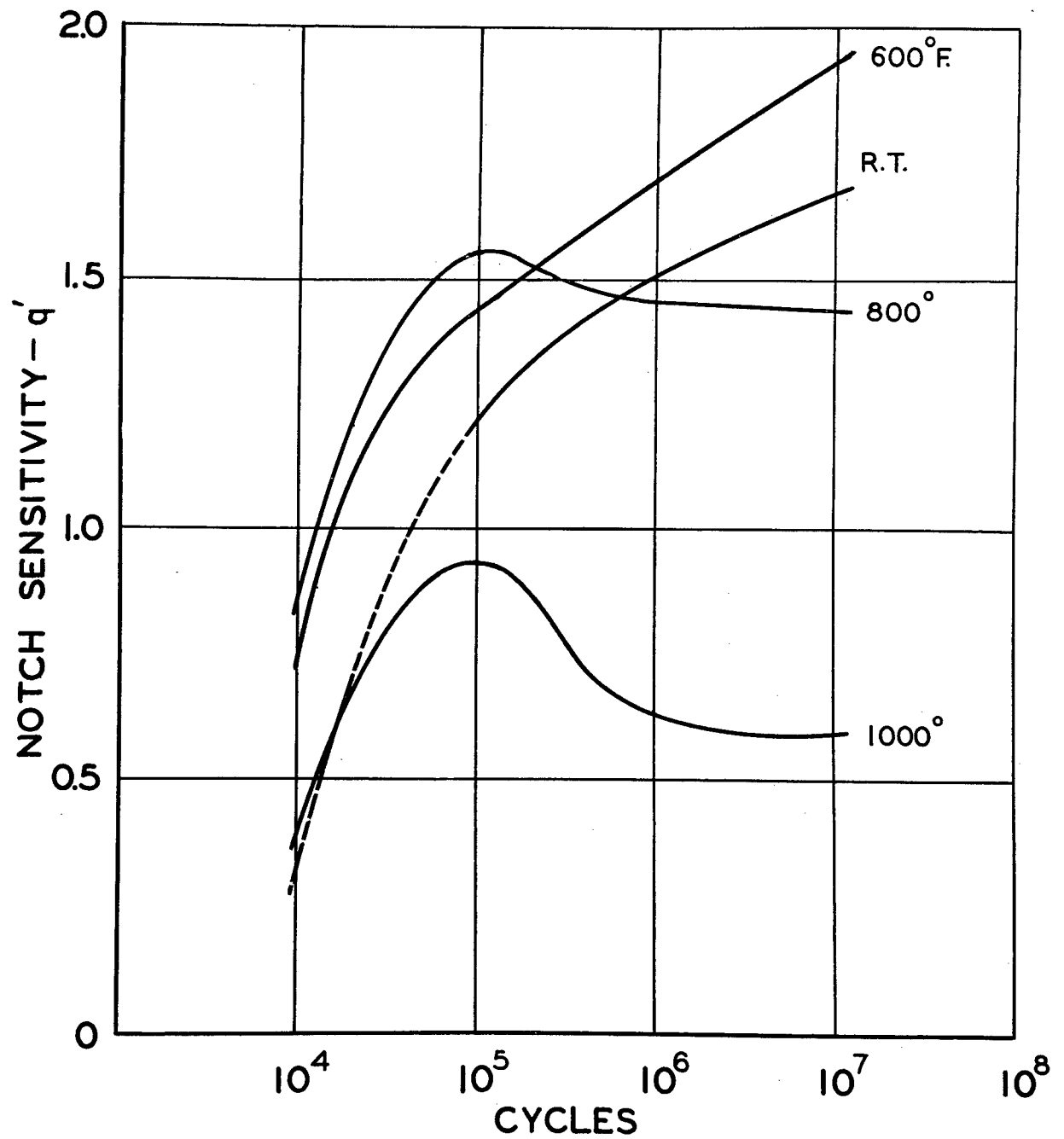
FIG. 34. FATIGUE NOTCH SENSITIVITY AS FUNCTION OF LIFE FOR ROOM
AND ELEVATED TEMPERATURES, COMPLETELY REVERSED
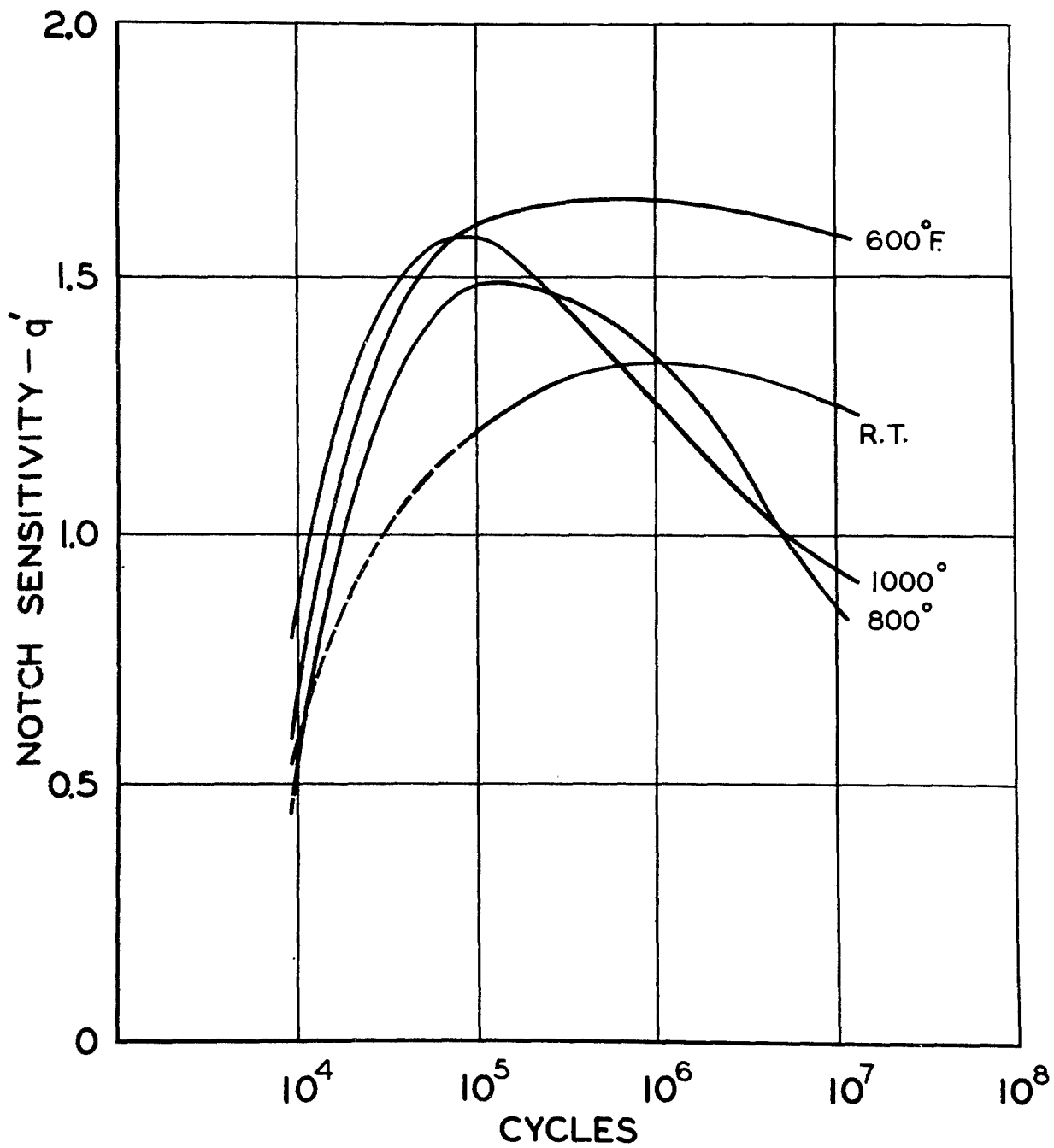
FIG. 35. FATIGUE NOTCH SENSITIVITY AS FUNCTION OF LIFE FOR ROOM
AND ELEVATED TEMPERATURES, TENSION, ZERO TO MAXIMUM
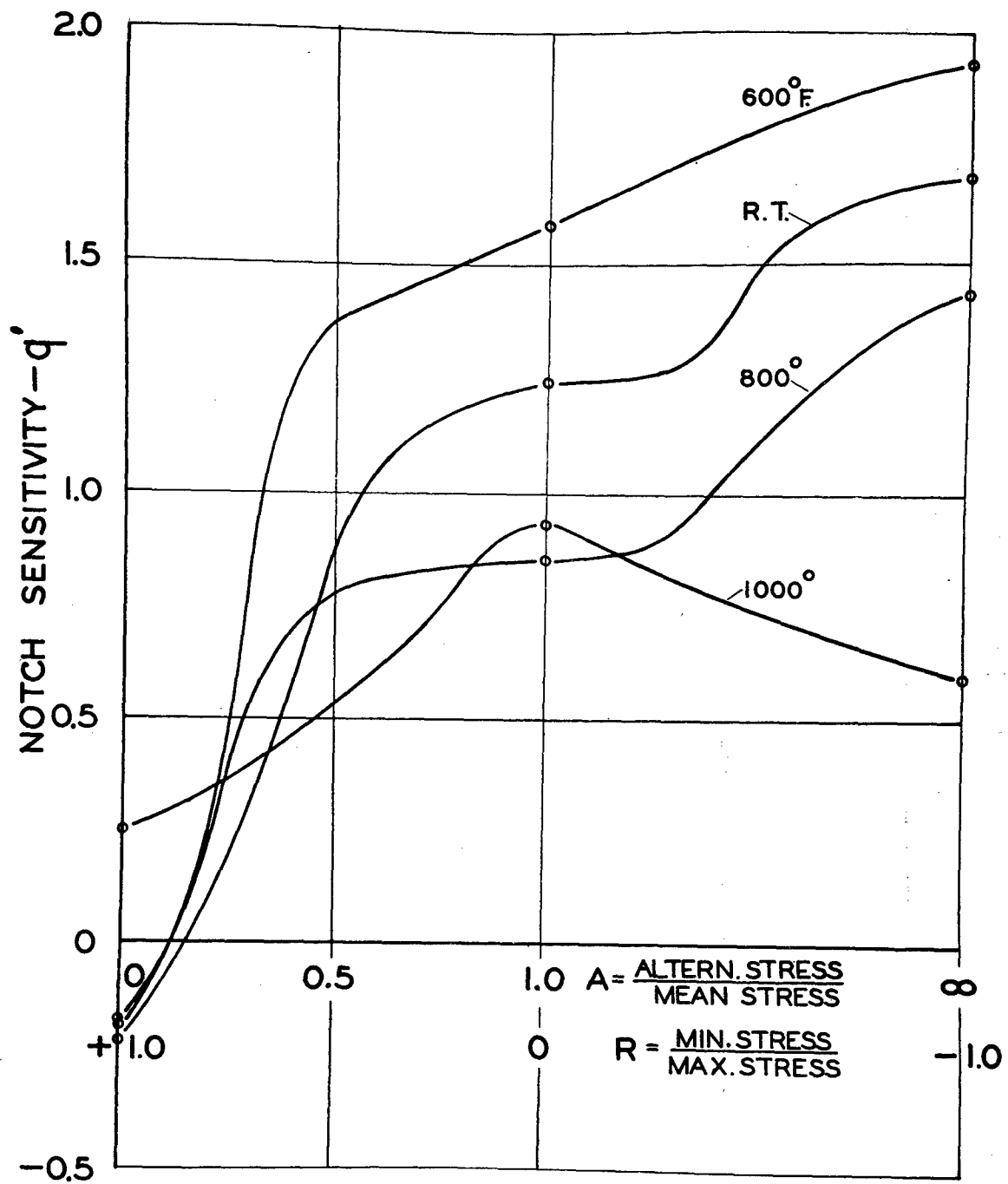
FIG. 36. FATIGUE NOTCH SENSITIVITY AS FUNCTION OF STRESS RATIO
FOR ROOM AND ELEVATED TEMPERATURES

$S_c = 52,000$ psi
$A = 0$ | $\varepsilon = 32\%$

$S_m = 50,000$ psi
$S_{max} = 63,000$ psi
$A = 0.26$ | $\varepsilon = 16\%$

$S_m = 42,000$ psi
$S_{max} = 78,000$ psi
$A = 0.85$ $\varepsilon = 4\%$

$S_m = 34,250$ psi
$S_{max} = 68,500$ psi
$A = 1.0$ | $\varepsilon = 2.7\%$

$S_m = 0$
$S_{max} = 40,000$ psi
$A = \infty$ | $\varepsilon = 0.1\%$

TIME—HOURS
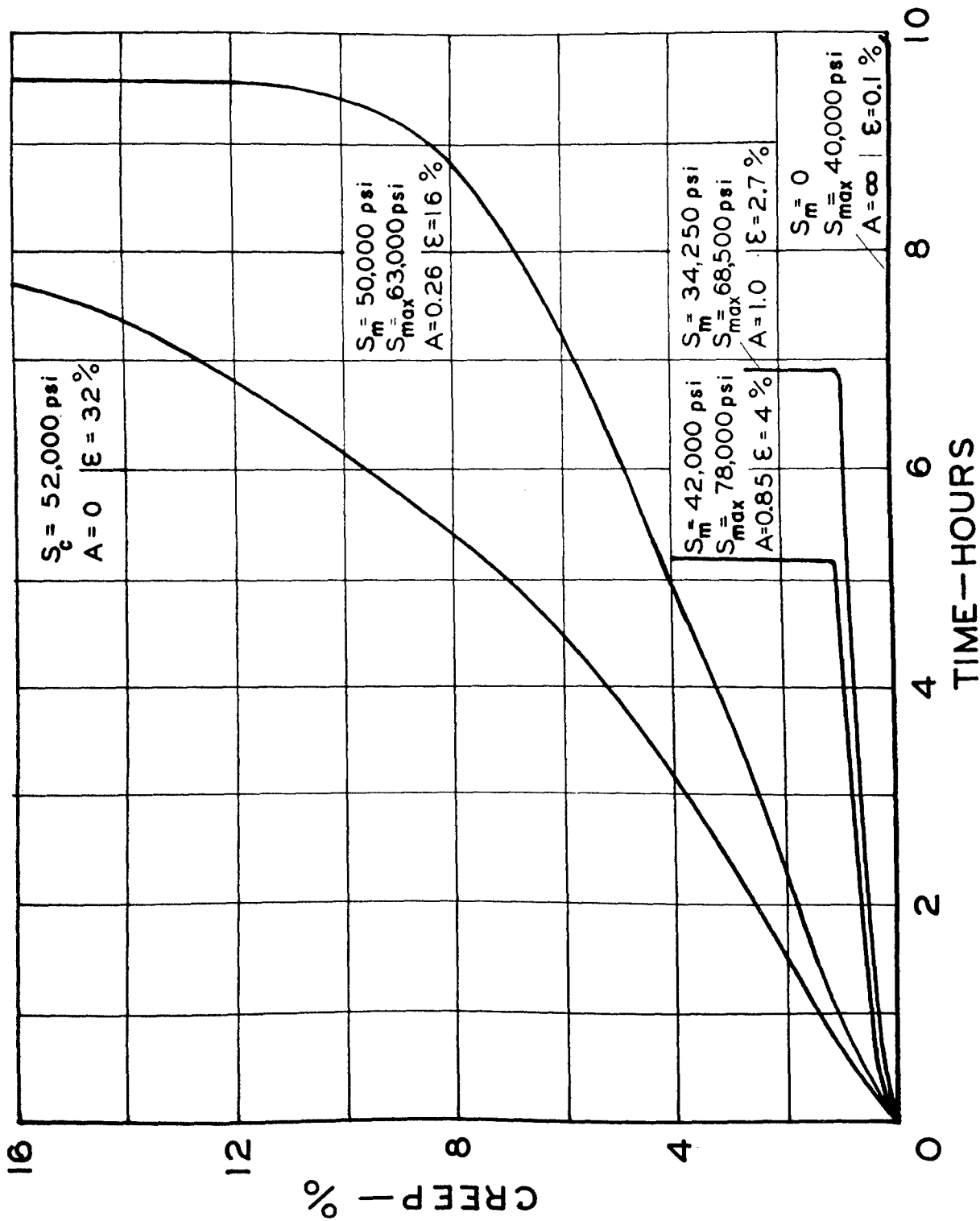
CREEP—%

FIG. 37. CREEP TIME DIAGRAMS, EFFECT OF MEAN STRESS ON CREEP AT 1000° F., UNNOTCHED
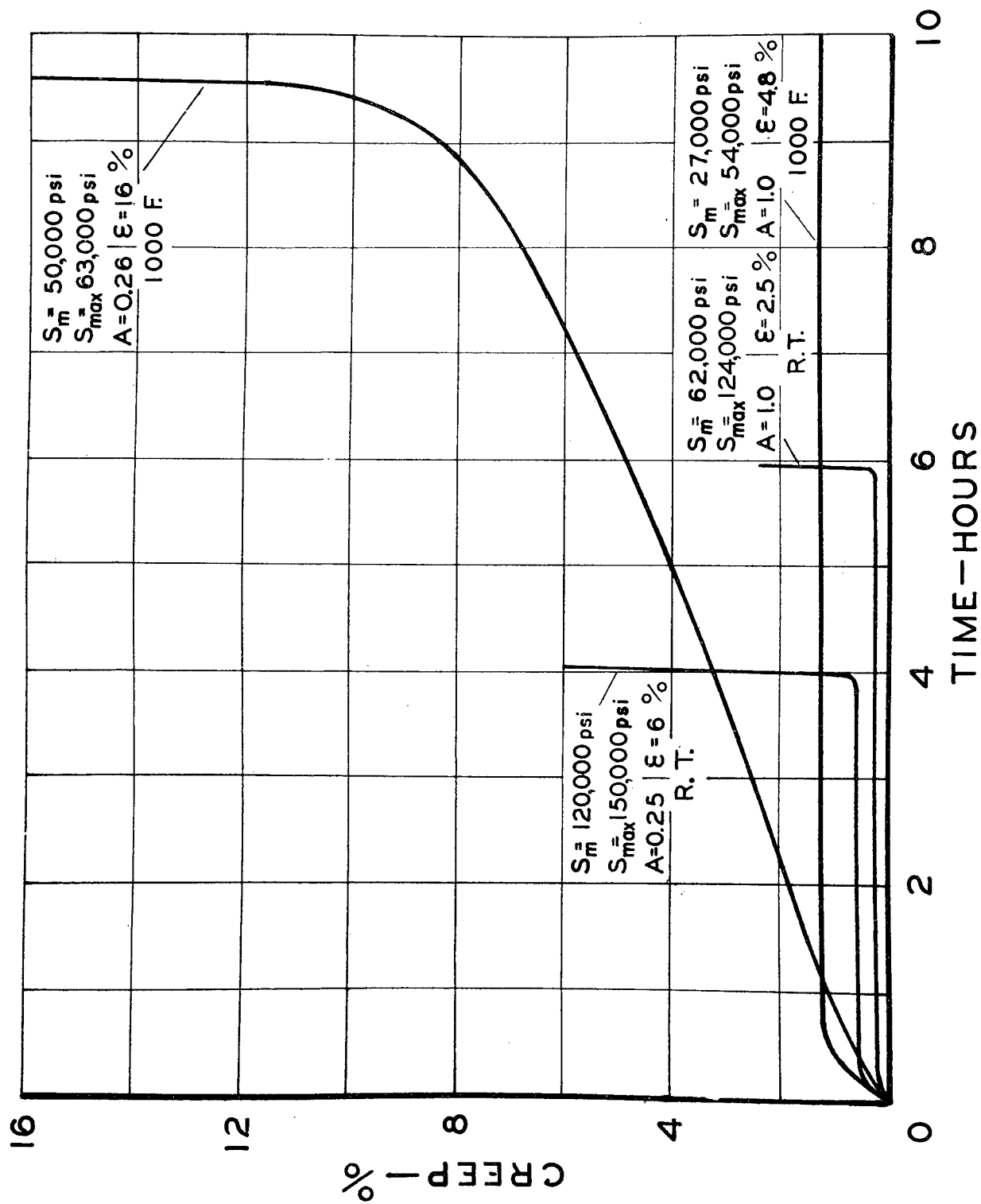
FIG. 38. CREEP TIME DIAGRAMS, EFFECT OF TEMPERATURE ON CREEP FOR TWO DIFFERENT STRESS RATIOS, UNNOTCHED
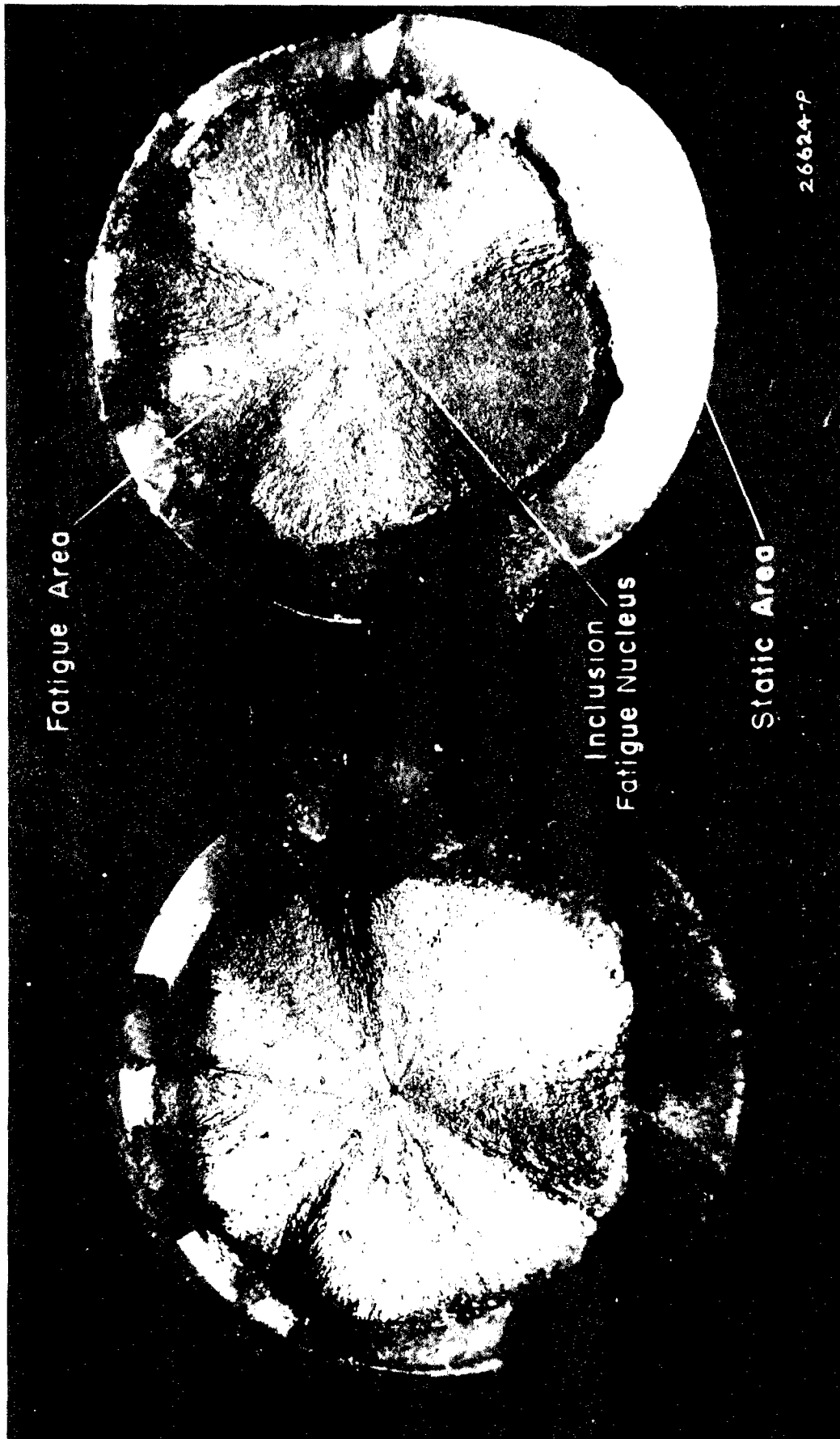
FIG. 39. FATIGUE FRACTURE WITH GLOBULAR INCLUSION AS NUCLEUS